

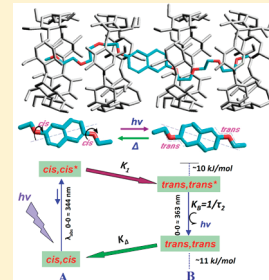
Controlling the Stereospecificity of a Volume-Conserving Adiabatic Photoisomerization within a Nanotubular Self-Assembled Cage: A Reversible Light–Heat Torque Converter

Ioanna Balomenou, Antonia Kaloudi-Chantzela, Nikolaos Karakostas, Konstantina Yannakopoulou, Irene M. Mavridis, and George Pistolis*

NCSR “Demokritos” Institute of Physical Chemistry, 153 10 Athens, Greece

 Supporting Information

ABSTRACT: We present herein a host–guest supramolecular system by which we were able to obtain precise control of the stereospecificity of a new and unusual adiabatic photoisomerization reaction capable of restoring reversibly the original configuration. The host–guest system is composed of (a) a naphthalene ring linked centrosymmetrically—via sp^2 hybridized oxygen atoms—with methoxytriethyleneglycol chains (**1**) and (b) a nanotubular cage formed by four self-assembled face-to-face β -cyclodextrins threaded onto the long “axle” of **1**. The compound **1** can exist in distinct *cis,cis*, *cis,trans*, and *trans,trans* conformations that are spectrally distinguishable (see Scheme 1). Spectroscopic and kinetic manifestations of the torsional isomerization of **1** in the lowest excited singlet state both in solution and within the tubular cage were investigated. The results provide clear evidence that the compact cavity completely blocks the photoisomerization pathway manifested in common solution (*cis,cis** → *cis,trans**), allowing observation of stereospecific, volume-conserving turning of the naphthalene ring about the two “quasidouble” bonds C_{Naph}–O by $\phi \approx 180^\circ$ (*cis,cis** → *trans,trans**). The photoisomerization is purely adiabatic, and the encaged molecule restores its original configuration by generating torque thermally, when relaxing to the ground state.



INTRODUCTION

There has been much discussion on how supramolecular effects dictate the course of photophysical and photochemical relaxation of organic molecules.^{1–4} Medium-controlled *cis/trans* geometric photoisomerizations are of particular importance as, besides the tremendous importance for understanding and mimicking natural photoprocesses,^{2,5–9} they could also be seen as a particularly powerful platform in the development of artificial molecular-level systems capable of harnessing motion for possible applications.^{10–18}

It is generally accepted that photochemical isomerization of unsaturated compounds such as olefins^{19–22} and polyenes²³ in uninhibited fluid media usually involves the large amplitude motion of a bulky group twisting about a C=C “axle”, namely, torsional relaxation or one-bond flip (OBF). In volume-confining media such as organic glasses, crystals, cavitands, and proteins’ pockets—where the volume-demanding OBF mechanism is blocked—the photoisomerizations are believed to proceed by small amplitude torsional flexibility of the isomerizing moiety,^{2,23} that is, concerted rotation—not necessarily synchronous^{5–7}—about more than one bond in a manner to minimize volume requirements. Recent computational studies, however, suggest that a volume-saving motion may be possible in the absence of a restricted medium.⁶ The rotating bonds may be either alternating double bonds or a pair of adjacent double and single bonds. The former is related to the “crankshaft” motion and is known as the bicycle-pedal (BP) mechanism;^{24–29} simultaneous three-bond

cis-trans photoisomerizations, termed also as asynchronous double bicycle-pedal deformations of a conjugated moiety, have been suggested recently.^{8,9} The latter concerted rotation process involves out-of-plane transportation of the C–H unit in a double bond of the polyene skeleton, the so-called hula-twist (HT) motion.^{23,30–35} The involvement of related photoisomerization processes in confined spaces has also been suggested for organic compounds bearing heteroatomic double bonds C=N (e.g., photochromic salicylideneanilines)³⁶ and quasi-single bonds such as C::S (thiocinnamate chromophore in the binding cavity of the photoactive yellow protein (PYP)).²³ It is also proposed that chromophores bearing lone-pair electrons ($n \rightarrow \pi^*$ transitions), such as azomethines ($R_1R_2C=N-H$) and the related azobenzenes,³⁷ undergo diabatic *cis-trans* photoisomerization, which is possibly driven by an inversion process centered at the nitrogen atom.

The above one-photon, two-bond twisting isomerization processes are in general associated by *adiabatic* pathways. That is, the overall reaction course includes principally two trajectories (one for each surface, i.e., S_1 and S_0) linked by a radiationless transition through the S_1/S_0 conical intersection (CI). It is not at all clear whether the isomerization is completed purely in S_1 or proceeds primarily in the thermal ground state potential surface (S_0).

Received: April 22, 2011

Revised: August 1, 2011

Published: August 03, 2011

It is generally suggested that the S_1 twisted intermediate is funneled through the CI to the ground surface where both bonds relax, rotating continuously until reaching the final stable configuration(s).

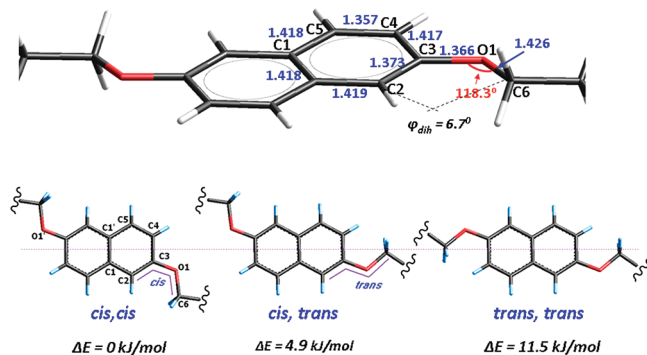
While successful attempts have been made to harness volume-demanding rotary motion in a reversible manner^{10–18}—via rotation about the C=C axle of a bulky molecular subunit—the realization of similar behavior for *volume-preserving* motions remains unexploited. This concept lies beyond the above-mentioned conventional one-bond-twist (C=C) photoisomerization scheme and could form the basis for converting light into molecular mechanical motion operating reversibly with no volume displacement (such as the turning of a molecular subunit shaped like a cylinder along two bonds linked centrosymmetrically to the stator moiety, up to date feasible only thermally^{38–40}). Unfortunately, the presence of more than one trajectory and the increased torsional flexibility associated with volume-conserving *adiabatic* photoisomerizations usually lead to conformationally stable products (in S_0) energetically unable to restore the original configuration.

The challenging work, therefore, we have to do is to create a unique cavity around the photoreactive guest, tailored to afford steric inhibition on selective torsional motion(s) while leaving as much free-volume compartments as possible near the tested photoreactive site. Fine tuning of the blocking space around the reactive center would allow one to obtain precise control of the stereospecificity of a certain reaction coordinate capable of reversibly restoring the original configuration. Some *adiabatic* photoisomerization reactions may possibly be attractive candidates for this purpose. Adiabatic photoreactions⁴¹ are known to proceed through a single trajectory purely in S_1 . For these reactions, the absence of the conical intersection eliminates many complications associated with electronically diabatic effects (such as photobleaching or creation of additional ground-state stable photoproducts) and allows for *direct* elucidation of the isomerization coordinate by straightforward fluorescence kinetic analysis.

Recent studies by us^{42,43} and others⁴⁴ provide evidence that 2-methoxyanthracene, 2-methoxynaphthalene,⁴² and its 2,6-disubstituted related derivatives⁴³ **1** and **2** (Schemes 1 and 2) undergo *adiabatic* photoisomerization in the first excited state (S_1). Owing to the fact that the $C_{\text{Naph}}-\text{O}$ linking demonstrates substantial double-bond character,⁴⁵ the above materials can exist in planar, spectrally discrete *cis* (*syn*, $\varphi = 0^\circ$) and *trans* (*anti*, $\varphi = 180^\circ$) rotational isomers which differ noticeably in energy in the S_0 (see Schemes 1 and 2). The planar *cis* geometric isomers are the energetically preferred configurations—in consistency with theory—and were the only forms observed in the crystal structure of both 2-methoxynaphthalene⁴⁶ and 2,6-dimethoxytriethyleneglycol naphthalene⁴⁵ (**1**). Spectroscopic and kinetic manifestation of the adiabatic isomerization of **1** and **2** in solution suggests that, at least for **1**, the *cis,cis** \rightarrow *cis,trans** isomerization proceeds through a volume-conserving pathway, involving most likely *out-of-plane* inversion in one of the two sp^2 hybridized oxygen atoms.⁴³

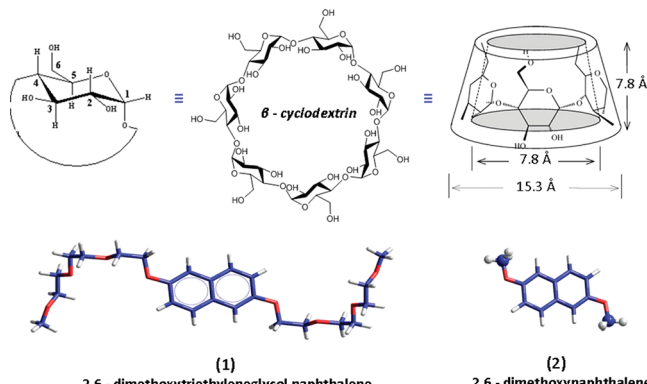
Recognizing the well-known ability of polymeric glycols to thread onto their long axle cyclodextrins giving polyrotaxanes,^{47–54} we reasoned that the encirclement of **1** by the tight tubular cage formed from assembled β -cyclodextrins (β -CDs) might reveal new and unusual, otherwise nonpreferred, stereospecific structural rearrangement. Observations reported here show that irradiation of encapsulated **1** results in *adiabatic* rotation of the naphthalene ring in S_1 about the two $C_{\text{Naph}}-\text{O}$ axles by $\varphi \sim 180^\circ$. When relaxing to the ground state, the molecule is rewound

Scheme 1. (Top) X-ray *cis,cis* Core Structure of **1** and **(Bottom)** Ground State Core Structures and Relative Energies of the Distinct Stereoisomers of **1** Obtained Experimentally and Supported Also Computationally^{45,a}



^a The *cis* (*syn*, $\varphi \approx 0^\circ$) and *trans* (*anti*, $\varphi \approx 180^\circ$) planar configurations are denoted by the dihedral angle φ ($\text{C}_2-\text{C}_3-\text{O}_1-\text{C}_6$) formed by the naphthalene plane and the O_1-C_6 bond vector.

Scheme 2. Host–Guest Materials Used in This Work



thermally generating torque to restore the original (*cis,cis*) configuration. The engaged molecule then behaves as a reversible light–heat torque converter. To our knowledge, this is the first observation of simultaneous nonadjacent *two-bond-twist* photoisomerization in the adiabatic excited state surface.

■ RESULTS AND DISCUSSION

Part A. Complexation Studies in Solution. There are several reports on the formation of rotaxanes upon reaction of oligo- or poly(ethylene glycols) with cyclodextrins (CDs) in water.^{47–54} Confirmatory structural information hitherto is given by an available crystal structure⁵⁵ which consists of a poly(ethylene glycol) chain threaded through hydrogen-bonded head-to-head dimers of β -CD. Taking advantage of the above facts and the well-known property of the cyclodextrin cavity to attract small aromatic molecules,^{53,54} we synthesized compound **1** tailored to facilitate threading of up to four β -CD units upon properly adjusting the mixing ratio of the reactants, i.e., **1** and β -CD, in water (vide infra).

1. ^1H NMR and 2D DOSY Spectra. (a). ^1H NMR. Initial complexation studies were performed using an ^1H NMR titration

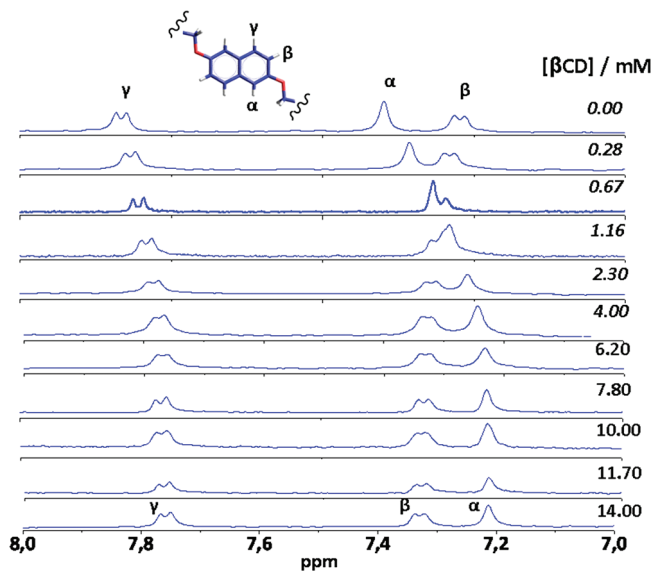
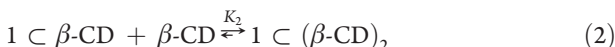


Figure 1. Partial ^1H NMR spectra from the addition of β -CD to **1** ($80.0 \mu\text{M}$) in D_2O .

with $[1] = 80.0 \mu\text{M}$ vs $[\beta\text{-CD}]$. The results show clear indication of binding. We should note that we mainly focused on the chemical shift changes of the aromatic region of the spectrum of **1**, as the part of the methoxytriethyleneglycol subunit was too crowded for analysis due to strong overlap with the signals of the cyclodextrin macrocycle (for the assignment of all proton signals see the 2D HSQC spectrum in the Supporting Information). Sequential β -CD additions cause systematic perturbation of the chemical shift of the aromatic protons as shown in Figure 1. Saturation is soon observed above $[\beta\text{-CD}] \approx 2.30 \text{ mM}$. The changes of δH_{naph} with increasing $[\beta\text{-CD}]$ are initially sharp and then are steeply curved and soon level-off. These particular features are highly consistent with the presence of consecutive steps^{56,57} of complexation between **1** and β -CD. To elucidate the stoichiometries and to extract numerical values for the association constants K_j involved in the successive formation of the growing assembly, we have made extensive use of computer fits and simulations, and the concentrated results are discussed below in terms of all possible stoichiometries of complexation.

The complexation scheme of threading **1** through β -CD macrocyclic rings can be modeled to proceed as an associative chain reaction, each step of which consists of the attachment of one β -CD unit to the growing assembly. The steps therefore that lead to the formation of the above superstructures can be described by the following eqs 1–4



The possible stoichiometries and the associated binding constants (K_j) were tested by fitting directly the experimental

data δH_{naph} vs $[\beta\text{-CD}]$ to the master eq 5 as the case may be ($j = 1–4$).

$$\delta_{\text{obs}} = f_{\text{free}}\delta_{\text{free}} + \sum_{j=1}^{j=4} f_{1j}\delta_{1j} \quad (5)$$

$$f_{1j} = \frac{[1 \subset (\beta\text{-CD})_j]}{[1]_{\text{tot}}} \quad (5a)$$

In the above model, δ_{obs} is the observed chemical shift of an aromatic proton at any moment during the titration procedure. δ_{1j} and f_{1j} represent the chemical shift and the molar fraction of the various $1 \subset (\beta\text{-CD})_j$ adducts, respectively, and $[1]_{\text{tot}} = 80.0 \mu\text{M}$ is the total concentration of **1**. δ_{free} stands for the chemical shift of the free (uncomplexed) **1** before any addition of β -CD, and f_{free} is the molar fraction of the free **1** that remains uncomplexed at any moment during the titration.

Assuming the simplest case, i.e., the formation of only 1:1 adducts ($1 \subset (\beta\text{-CD})$), and setting $\delta_{11} = 7.34 \text{ ppm}$ (H_β) (obtained from the leveling off part of the experimental curve), the model (eq 5; $j = 1$) failed significantly to give an acceptable fit ($R^2 = 0.993$; see Figure 2a). We have further increased the number of the free-running parameters of eq 5, hypothesizing that the assembly is terminated with the formation of the $1 \subset (\beta\text{-CD})_2$ entity. Because of (a) the high symmetry of the above supramolecular adduct and (b) the fact that two face-to-face β -CDs can encircle completely the aromatic ring, the leveling off value of the experimental curve (i.e., 7.34 ppm) was taken into account for the chemical shift of the H_β protons in the fully complexed state, i.e., $1 \subset (\beta\text{-CD})_2$; furthermore, we set $\delta_{12} \approx 2 \delta_{11}$ to the fitting eq 5; $j = 2$. In spite of the increased number of parameters (i.e., K_1 and K_2), the respective model was still unable to fit the steeply curved part of the data ($R^2 = 0.996$), as clearly seen in Figure 2b.

On the basis of (a) the poor fits obtained above and (b) the geometrical features of compound **1** tailored to afford threading along its elongated dimension of up to four β -CD units, it is conceivable, in principle, to account for the presence in the solution of all the possible stoichiometries, i.e., $1 \subset (\beta\text{-CD})_j$ with $j = 1–4$. Steps 3 and 4 can be considered to proceed through the successive attachment of a β -CD molecule at each of the ends of the $1 \subset (\beta\text{-CD})_2$ adduct. The precursory $1 \subset (\beta\text{-CD})_2$ entity is centrosymmetric, and therefore, one would expect the above steps (i.e., 3 and 4) to have similar binding strength, i.e., $K_3 \approx K_4$. Furthermore, the presence of the above terminal binding steps should in fact not be affecting the chemical shift of the protons of the core naphthalene ring. The justification for this hypothesis rests on the fact that in both steps (3 and 4) the attached macrocycles (β -CD) encircle the ends of the oligomeric chains of **1**. Therefore, perturbation of the δH_{naph} is not typically expected to occur since the interspace contacts ($\sim 10 \text{ \AA}$) between the end-attached β -CDs and the aromatic core exceed the NMR detection limit ($\leq 5 \text{ \AA}$). We can therefore suggest that only the first two building steps, i.e., (1) and (2), dominate the δH_{naph} vs $[\beta\text{-CD}]$. Nevertheless, the presence of the equilibria (3) and (4)—albeit not affecting the δH_{naph} —implicitly plays a crucial and definitive role in the formation of the steeply curved features of the δH_{naph} vs $[\beta\text{-CD}]$. This can be easily understood if one considers the chain reaction described by eqs 1–4. If the terminal steps 3 and 4 are thermodynamically favored, then as the concentration of β -CD sequentially increases the equilibria progressively move toward formation of the largest superstructure,

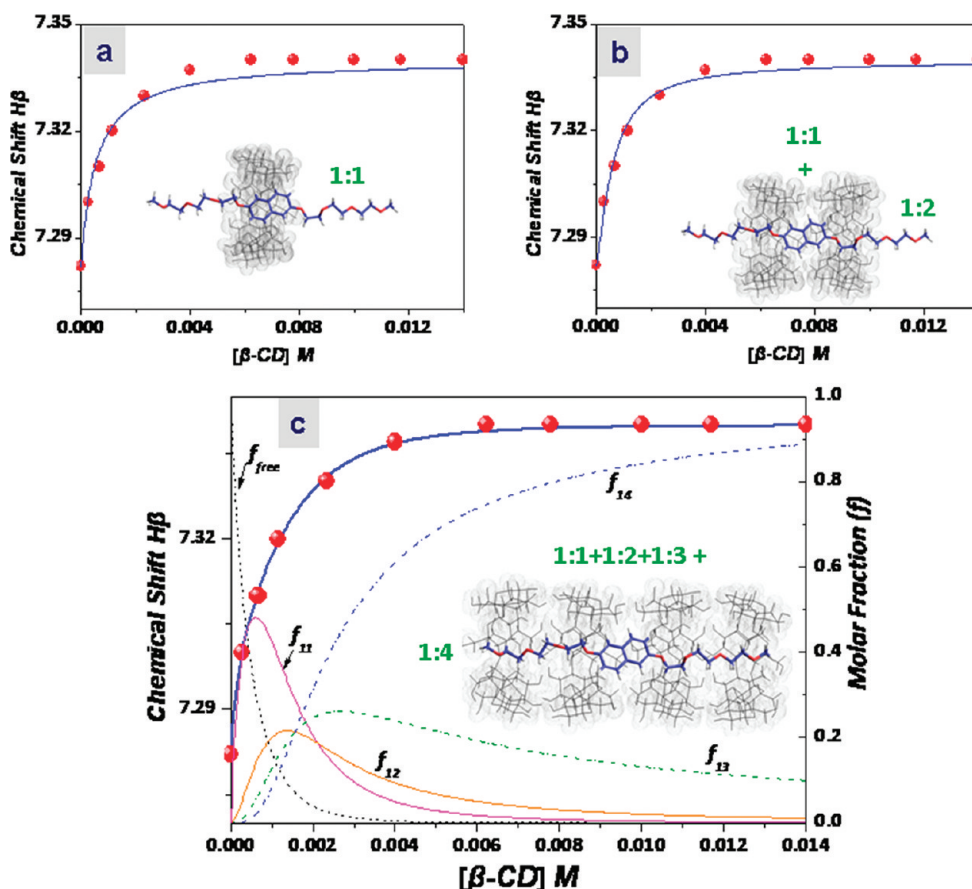


Figure 2. Computer fits (solid lines) of eq 5 to the δH_β vs $[\beta\text{-CD}]$ experimental data (red circles) for successive steps of complexation between **1** and $\beta\text{-CD}$. (c) Plot of the molar fractions ($f_{1j}; j = 1\text{--}4$) of the species involved in the fit. For fitting parameters and goodness of the fits, see Table 1.

i.e., **1** $\subset (\beta\text{-CDs})_4$. This causes in turn the concentration of the small and medium-sized adducts (i.e., **1**_{free}, **1** $\subset \beta\text{-CD}$, and **1** $\subset (\beta\text{-CD})_2$) to vanish sharply as it is clearly indicated by the variation of the molar fraction of each of those complexes with $[\beta\text{-CD}]$ (see $f_{1j}; j = 1\text{--}4$ in Figure 2c). These aspects of coupled equilibria should in fact regulate the sharply curved features of the δH_{Naph} vs $[\beta\text{-CD}]$. Parenthetically, we may note that such distinctive features (i.e., sharp rise and fast leveling off of the experimental curve) were proven to be highly diagnostic for the formation of large nanotubular assemblies formed between cyclodextrins and certain rodlike molecules via a self-associative chain reaction in aqueous solutions.^{56,57}

To check the plausibility of the above interpretation, we have fitted δH_β vs $[\beta\text{-CD}]$ using the complete eq 5 ($j = 4$). We have further made the hypothesis that $K_1 \neq K_2 = K_3 = K_4$ to maintain the number of the free-running parameters equal to 2, as with the case of eq 5 ($j = 2$) shown in Figure 2b by which the fit was not acceptable. We have obtained for δH_β vs $[\beta\text{-CD}]$ the fit shown in Figure 2c with a very satisfactory criterion for its goodness of fit (see Table 1). The above provide conclusive evidence that the incorporation of steps 3 and 4 into the fitting of eq 5 (i.e., the formation of the largest adducts) is critical for the experimental data to be fitted satisfactorily. Finally, using eq 5 ($j = 4$) and allowing three free-running parameters, i.e., K_1 , K_2 , and $K_3 = K_4$, to the minimization progress, we have also obtained a unique fit, but no improvement of the correlation of the parameters was achieved (see Table 1). The results in general show—with the exclusion of the initial step 1—that the associative chain reaction

proceeds with steps all of which have similar association constants. Similar results were obtained when δH_α or δH_γ vs $[\beta\text{-CD}]$ were used for the estimation of the binding constants.

(b). *2D DOSY Spectra.* 2D diffusion-ordered NMR studies yielded information on the relative sizes of the solutes. A comparison was made between the translational diffusion coefficients (D) of two samples (in D_2O at 298 K) containing an equimolecular amount of $\beta\text{-CD}$: one of $\beta\text{-CD}$ alone (12.0 mM) and the other in the presence of 1.0 mM of the guest **1**. For the host $\beta\text{-CD}$ alone a $D = 1.62 \pm 0.11 \times 10^{-10} \text{ m}^2/\text{s}$ was measured (see Figure 3). This value is close to those reported in the literature^{58,59} considering the weak dependence of D upon concentration of $\beta\text{-CD}$ ($D = 3.29 \pm 0.07 \times 10^{-10}$ and $2.71 \pm 0.05 \times 10^{-10} \text{ m}^2/\text{s}$ for 0.5 and 8 mM solutions, respectively, of $\beta\text{-CD}$ in D_2O at 298 K). For a sample containing 1.0 mM **1** and 12.0 mM $\beta\text{-CD}$, the DOSY spectrum reveals a single band corresponding to an average diffusion coefficient of $D = 0.38 \pm 0.04 \times 10^{-10} \text{ m}^2/\text{s}$. This value is nearly 4-fold smaller compared to that obtained with $\beta\text{-CD}$ alone (12.0 mM) and indicates that the composition of the solution is dominated by the largest **1** $\subset (\beta\text{-CDs})_4$ adduct. It is important also to note that the guest (**1**) diffuses together with the assembled $\beta\text{-CDs}$ as clearly demonstrated by the aromatic region of the ^1H DOSY spectrum. Calculations using the binding constants obtained from the best fit of δH_{Naph} vs $[\beta\text{-CD}]$ confirm the predominance of the **1** $\subset (\beta\text{-CDs})_4$ adduct in the above sample. These findings are in consistency with the predictions of the Stokes–Einstein equation in which D is inversely

Table 1. Binding Constants Extracted from Fits of δH_p vs $[\beta\text{-CD}]$ of the Various Tested Stoichiometries of Complexation Between **1** and β -Cyclodextrin in D_2O

stoichiometry of the assembly	binding constants (M^{-1})	goodness of the fit, R^2
1 $\subset \beta\text{-CD}$	$K_1 = 1890 \pm 290$	0.991 (Figure 2a)
1 $\subset \beta\text{-CD}$	$K_1 = 1570 \pm 500$	0.996
1 $\subset (\beta\text{-CDs})_2$	$K_2 = 1600 \pm 460$	(Figure 2b)
1 $\subset \beta\text{-CD}$	$K_1 = 3890 \pm 290$	0.9996
1 $\subset (\beta\text{-CDs})_2$	$K_{2=3=4} = 410 \pm 16$	
1 $\subset (\beta\text{-CDs})_3$		(Figure 2c)
1 $\subset (\beta\text{-CDs})_4$		
1 $\subset \beta\text{-CD}$	$K_1 = 4200 \pm 500$	0.9996
1 $\subset (\beta\text{-CDs})_2$	$K_2 = 360 \pm 80$	
1 $\subset (\beta\text{-CDs})_3$	$K_{3=4} = 475 \pm 110$	(Figure 2c)
1 $\subset (\beta\text{-CDs})_4$		

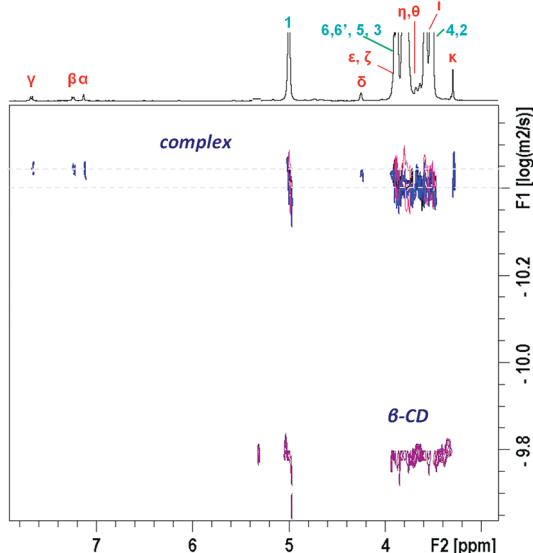


Figure 3. 500 MHz ^1H DOSY spectra of β -CD alone (12.0 mM) and in the presence of the guest **1** (1.0 mM) in D_2O at 298 K. (For the assignment of the hydrogens of β -CD, see Figure 6, and for **1** see Supporting Information Figure S1).

proportional to the hydrodynamic radius r or, approximately, to the molecular weight of the solute.

II. Time-Resolved Fluorescence Anisotropy. Perhaps the most powerful and accurate method to verify the average molecular weight of assembled fluorescent nanostructures in dilute solutions is the depolarization of the emission, frequently expressed in terms of the loss of the fluorescence anisotropy $r(t)$ as a function of time. When a proper fluorophore is tightly restricted in the environment of a host (e.g., a cyclodextrin cavity), it typically rotates as a whole with the host molecule, and only a global tumbling motion is observed. This motion depends upon the size and shape of the rotating superstructure as well as the viscosity of the medium. The rotational correlation time τ_r of a solute can be accurately described by the modified

Stokes–Einstein–Debye (SED) hydrodynamic⁶⁰ eq 6

$$\tau_r = (fC) \frac{\eta V}{k_B T} \quad (6)$$

where V is the molecular volume; η is the viscosity of the solvent; k_B is the Boltzmann constant; T is the absolute temperature; f is the shape factor; and C is the boundary condition parameter which depends strongly on solute–solvent relative size. For the present system, we can set $C \approx 1$ (stick boundary condition) since the size of the possible rotating entities $\mathbf{1} \subset (\beta\text{-CDs})_j$ is considerably larger than that of the solvent molecules (water). The possible superstructures can be generally modeled as prolate ellipsoids of revolution. By applying the proper modifications to the shape factor f , the rotational diffusion time (τ_r) can be expressed⁶¹ by eq 7

$$\tau_r = \frac{2(\rho^2 + 1)(\rho^2 - 1)^{3/2}}{3\rho[(2\rho^2 - 1)\ln\{\rho + (\rho^2 - 1)^{1/2}\} - \rho(\rho^2 - 1)^{1/2}]} \frac{\eta V}{k_B T} \quad (7)$$

where ρ is the ratio of the longitudinal semiaxis α to the equatorial semiaxis b ($\rho = \alpha/b$), with $\alpha > b$ and $\alpha \approx b$ for a cylinder and a sphere, respectively. The absorption transition dipole $S_0 \rightarrow S_1$ of **1** is oriented along the minor molecular axis which coincides with the short symmetry axis of the ellipsoid. Furthermore, the emission dipole is nearly collinear with that of the absorption (the fundamental fluorescence anisotropy r_0 reaches the value of ~ 0.38 in frozen media where molecular tumbling is ceased; see Figure S4 in the Supporting Information). These features simplify the rotational depolarization analysis which was found to follow single exponential behavior with the instrumental setup used here.⁶²

For a sample containing **1** (78.0 μM) in the presence of a large excess of β -CD (12.0 mM), we have analyzed simultaneously the parallel and perpendicular polarized decay components of the emission (eqs 8a, 8b) to recover the intensity and anisotropy decay law.

$$I_{\text{VH}}(t) = A_{\text{VH}} + B_{\text{VH}}[1 - r_0 e^{(-t/\tau_r)}]e^{(-t/\tau_f)} \quad (8a)$$

$$I_{\text{VV}}(t) = A_{\text{VV}} + B_{\text{VV}}[1 + 2r_0 e^{(-t/\tau_r)}]e^{(-t/\tau_f)} \quad (8b)$$

The polarized decay laws for both crossed and parallel decays were used with the instrument response function to calculate the overall global minimum. The parameters, i.e., the rotational reorientation time (τ_r), the fluorescence lifetime (τ_f), and the initial anisotropy (r_0), were varied simultaneously⁶³ to obtain the best fit shown in Figure 4 with $\tau_r = 1.32 \pm 0.07$ ns, $\tau_f = 12.7 \pm 0.02$ ns, and $r_0 = 0.14 \pm 0.02$. The fit was highly reproducible, and three independent sets of experiments were carried out to determine the uncertainty which was found to be less than 5%.

Experimental evidence from the literature^{64,65} suggests that small adducts of 1:1 stoichiometry between fluorophores and β -CD in aqueous solutions rotate with subnanosecond correlation times, ca., $\tau_r = 0.3–0.5$ ns, in very good agreement with predictions of the SED eq 6. The present system is associated with a mean rotational correlation time of $\tau_r = 1.32$ ns. This is very close to the correlation time of the $\mathbf{1} \subset (\beta\text{-CDs})_4$ adduct as eq 7 predicts. More precisely, introducing $V = 3894 \text{ \AA}^3$ as the global volume for the above adduct (calculated by molecular modeling) and setting $\rho = \alpha/b \approx 31 \text{ \AA}/15 \text{ \AA} \approx 2$ into eq 7, we obtain $\tau_r = 1.44$ ns. It is worth noting that the experimentally

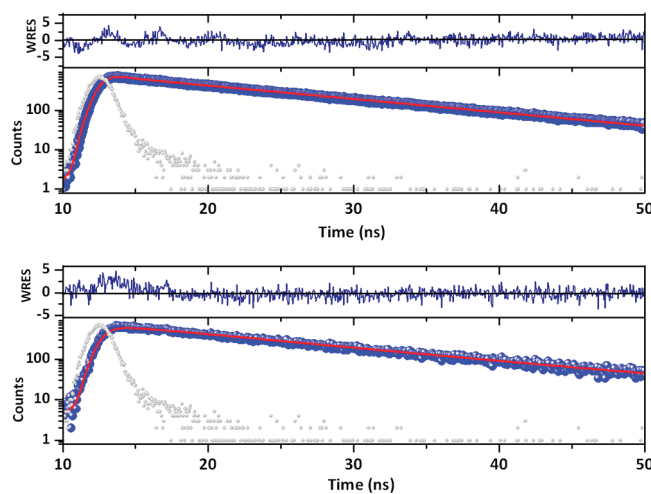


Figure 4. Simultaneous fit of both the parallel (up) and crossed (down) decay components of an aqueous solution of **1** ($78.0 \mu\text{M}$) containing $12.0 \text{ mM} \beta\text{-CD}$ at 296 K ; excitation at 340 nm . Emission observed at 380 nm with broad slits. Red solid line represents the best fitting curve. Gray curve is the instrument response function. The corresponding weighted residuals (WRES) are given on top for each curve (global $\chi^2 = 1.27$).

recovered value of $\tau_r = 1.32 \text{ ns}$ is well discriminated from that predicted for the close smaller $\mathbf{1} \subset (\beta\text{-CDs})_3$ assembly ($\tau_r \approx 1.0 \text{ ns}$). The above results are highly consistent with the NMR findings and strongly suggest that under a sufficient excess of $\beta\text{-CD}$ with respect to the guest **1** the composition of the solution is dominated by the largest assembly $\mathbf{1} \subset (\beta\text{-CDs})_4$.

III. Quenching Studies. To further prove the insulation and complete shielding of the fluorescent subunit by the threaded cyclodextrins, we have performed fluorescence quenching experiments using IO_3^- as a quencher. The bimolecular collisional quenching constant (k_q) was obtained from the slope of the Stern–Volmer plot

$$F_0/F = 1 + K_{sv}[Q] \quad (9)$$

according to the well-known relation

$$K_{sv} = k_q \tau_0 \quad (10)$$

F_0 and F are the fluorescence intensities in the absence and presence of quencher, respectively; τ_0 is the lifetime of the fluorophore in the absence of quencher; and Q is the concentration of quencher. As seen in Figure 5 when compound **1** and its less bulky analogue 2,6-dimethoxynaphthalene (**2**) are freely dissolved in an aqueous solution,⁶⁶ their own fluorescence is efficiently and almost equally quenched by IO_3^- . Both Stern–Volmer plots exhibit good linearity ($R^2 = 0.999$). The extracted K_{sv} values are nearly similar, i.e., 17.9 and 19.4 M^{-1} , for **1** and **2**, respectively, implying that the oligomeric chains of **1** barely affect the approach of the quencher to the fluorescent subunit. Similar results are obtained when τ_0/τ vs $[Q]$ is used, suggesting that the observed quenching is purely dynamic (collisional quenching). Combination of the above values with the lifetime of the emitting state $\tau_0 \approx 8.8 \text{ ns}$ demonstrates a k_q of about $2.3 \times 10^9 \text{ M}^{-1} \text{ s}^{-1}$: this approaches the diffusion limit in water⁶⁰ (near $1.0 \times 10^{10} \text{ M}^{-1} \text{ s}^{-1}$).

In obvious contrast to the freely dissolved derivatives of naphthalene, the encapsulated form of **1** is almost inaccessible to quencher as shown in Figure 5. By using $K_{sv} = 2.5 \text{ M}^{-1}$

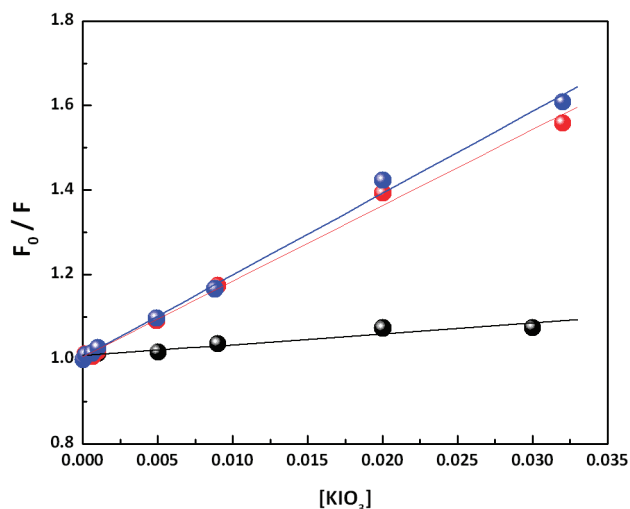


Figure 5. Stern–Volmer plots generated from fluorescence quenching at 380 nm in aqueous solutions of **1** (red circle), **2** (blue circles), and **1** ($78.0 \mu\text{M}$) in the presence of $12.0 \text{ mM} \beta\text{-CD}$ (black circle) using linear fits.

extracted from the fit and $\tau_0 \approx 13 \text{ ns}$, substitution into eq 10 yields $k_q \approx 2 \times 10^8 \text{ M}^{-1} \text{ s}^{-1}$ which is about 1 order of magnitude smaller than the diffusion-controlled value. The above results are in consistency with the NMR and fluorescence spectroscopy findings (vide infra) and clearly demonstrate that the core naphthalene subunit is well-fitted and efficiently shielded within the tubular cage.

IV. 2D NMR Spectroscopy/X-ray Crystallography. 2D rotating-frame nuclear Overhauser effect spectroscopy (ROESY) yielded quite detailed structural information about the supramolecular complex (Figure 6a). The collection of data was performed at ambient conditions using an aqueous solution with fixed concentration of $[\mathbf{1}] = 1.0 \text{ mM}$ and $[\beta\text{-CD}] = 4.0 \text{ mM}$. On the basis of the equilibrium constants obtained by the ^1H NMR titration method, calculations showed that the composition of the above solution is dominated by the large $\mathbf{1} \subset (\beta\text{-CDs})_j$ adducts, ca. $\sim 60\%$ ($j = 4$) and $\sim 25\%$ ($j = 3$), with only a minor contribution of the smaller-sized ones, ca. $\sim 10\%$ ($j = 2$) and $\sim 5\%$ ($j = 1$). The ROESY spectrum supports the structure shown in Figure 6b. Intermolecular cross peaks are observed between the aromatic protons of **1** and those of $\beta\text{-CD}$ located (a) inside the cavity, i.e., H_5 and H_3 , and (b) at the primary rim of $\beta\text{-CD}$ ($\text{H}_{6,6'}$). The involvement of protons of both sides of the naphthalene ring, i.e., H_α and H_γ , provides clear evidence of encapsulation. In general, the interactions of the aromatic hydrogens are considerably stronger with H_5 and $\text{H}_{6,6'}$ than with H_3 . This suggests encirclement of the aromatic ring by two face-to-face $\beta\text{-CDs}$ from their primary sides. The latter has been proven also by the crystal structure shown in Figure 6c. However, due to extensive disorder it has not been possible to determine the exact conformation of the long chain (vide infra). Encapsulation is further proven by the absence of cross peaks between aromatic protons and those (H_2 and H_4) of the exterior of the $\beta\text{-CD}$. Intramolecular contacts for **1** were also observed in the ROESY spectrum. As seen (Figure 6a), the exocyclic H_δ of **1** exhibits a strong cross peak with H_α and a considerably weaker one with H_β . The above findings strongly suggest the inclusion of the energetically preferred *cis,cis* configuration of **1** within the tubular cage. Further evidence is supplied in the optical spectroscopic section (Part B).

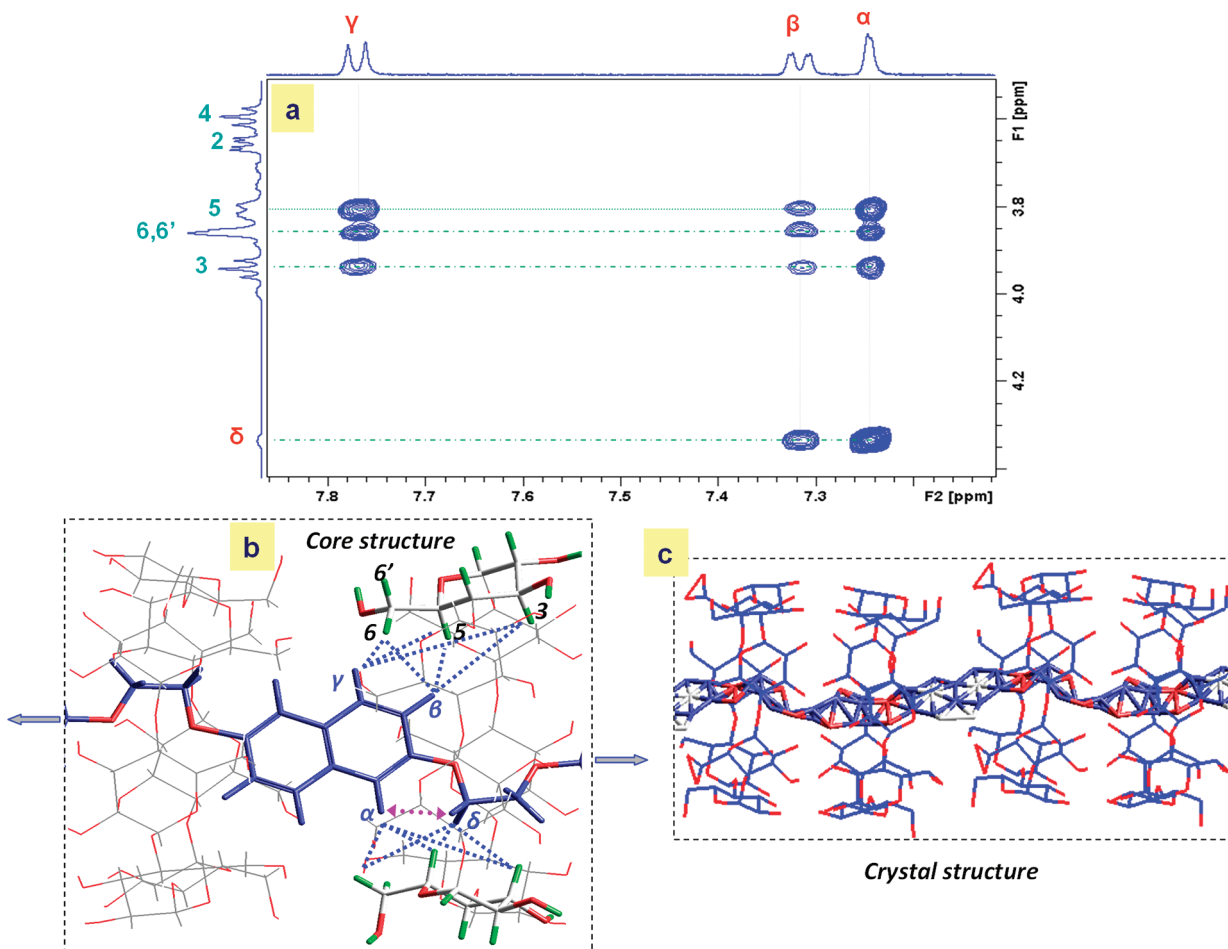


Figure 6. (a) Aromatic ROESY cross peaks observed for the complex between **1** and β -CD. (b) Core structure of the assembly in aqueous solution in the presence of a large excess of β -CD. Only half of the interactions between the members of the centrosymmetric system are shown. (c) Crystal structure of **1** \subset (β -CD)₄.

We have attempted also to crystallize the above complex by cooling slowly from ~ 60 °C to room temperature an aqueous solution containing the reactants in a mixing ratio of $\sim 1:4$. The X-ray structure was of low quality, and extensive disorder was observed within the cage (see Figure 6c). Nevertheless, the available data unambiguously proved the location of the guest **1** within the extended cavity formed by four self-assembled β -CD macrocycles (see Supporting Information for more details).

Part B. Photoisomerization of **1 in Solution (I) and within the Tubular Cage of the Assembled β -Cyclodextrins (II).** *I. In Solution.* The environment of a cyclodextrin cavity conceivably resembles that of cyclic ether. As the interest of this work focuses on exploring the photoisomerization behavior of **1** within the confined space formed by the hollow interior of the assembled cyclodextrins, we have herein investigated and compared the spectroscopy and kinetics of the adiabatic photoisomerization of **1** and **2**, dissolved in 2-methyltetrahydrofuran (2-MTHF). We have furthermore compared the results with those obtained in 3-methylpentane (3-MP) and in the more viscous tetradecane (C₁₄), as reported by us elsewhere.⁴³

Figure 7 displays the temperature dependence of the absorption spectrum of **1** and **2** in 2-MTHF upon cooling stepwise from 296 to 77 K. For comparison we present the temperature-dependent spectrum of **2** in 3-MP. As seen (Figure 7) at ambient

temperatures the predominant *cis,cis* form equilibrates thermally with the energetically closest lying *cis,trans* analogue ($\Delta E_{cc;ct} \approx 4\text{--}5$ kJ/mol), whose first absorption band appears as a weak shoulder at the red edge of the spectrum. Upon cooling stepwise, the shoulder gradually disappears, while several isosbestic points emerge across the absorption spectrum. Below ~ 130 K the equilibrium is practically shifted completely toward the thermodynamically stable *cis,cis* form.

The fluorescence spectra are more complicated and exhibit significant temperature-dependent features. At low temperatures, ca. below 260 K, the two isomeric forms, i.e., the *cis,cis** and *cis,trans**, do not interconvert in S₁; that is, each isomer decays itself with its own lifetime. This allows identification of their pure emission spectra after selective excitation as shown in Figure 8 (top). Above the temperature threshold of ca. 260 K, the barrier controlled, adiabatic isomerization rate constant in S₁ ($k_1 + k_{-1}$) becomes competitive with the decay constant of the excited state ($k_A = k_{f,A} + k_{nf,A}$; for an explanation of symbols, see Scheme 3). As a result, the isomers start to interconvert adiabatically in S₁ as manifested by both static and dynamic fluorescence spectroscopic analysis (vide infra).

As will be proven below by kinetic analysis, at ambient temperatures and above the interconversion process ($k_1 + k_{-1}$) becomes faster than the fluorescence decay (k_A). This is reflected

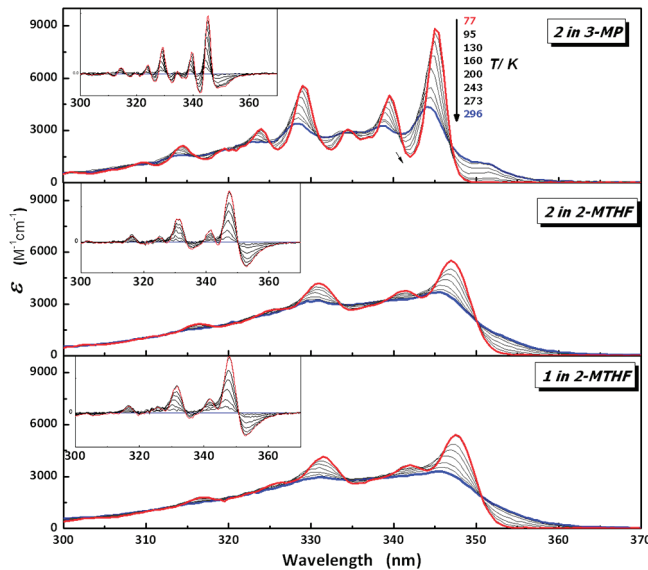


Figure 7. Absorption spectra of **2** in 3-MP (top) and 2-MTHF (middle) and **1** in 2-MTHF (bottom) at varying temperatures. Insets: Difference spectra (296 K) showing the isosbestic points.

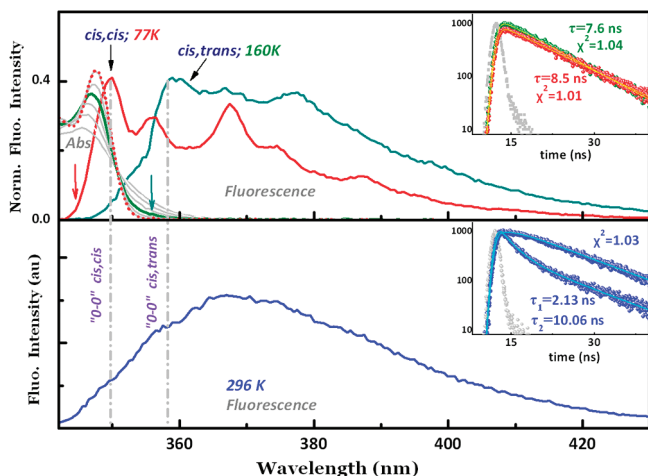
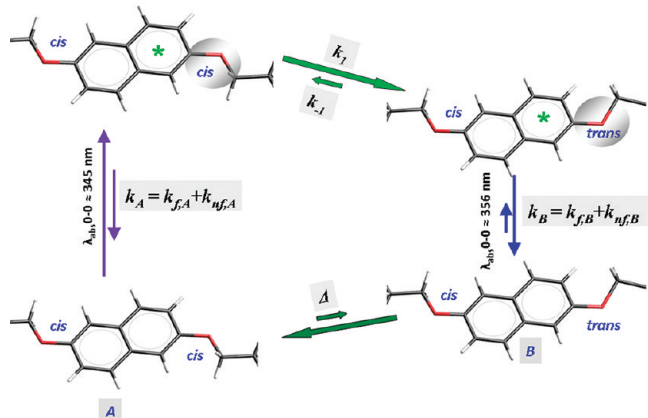


Figure 8. (Top) Pure emission spectra of the *cis,cis* and *cis,trans* isomers and fluorescence decays (inset) of **1** after selective excitation at low temperatures in 2-MTHF (see arrows). (Bottom) Room-temperature time-integrated (steady-state) fluorescence spectrum and wavelength-dependent decays (inset) after excitation (345 nm) of the predominant *cis,cis* form.

in the time-integrated fluorescence spectra which, actually, emanate from the equilibrium distribution of the emitting isomers in S_1 . Specifically, when the predominant *cis,cis* form is electronically excited at 296 K with continuous light (337 nm), the time-integrated fluorescence spectrum closely resembles that of the *cis,trans** isomer⁶⁷ (see Figure 8). It is clearly seen that the 0–0 vibronic band at 349 nm for *cis,cis** has decreased dramatically in intensity and was replaced by the 0–0 band at 358 nm for the *cis,trans** analogue. The fact that we see emission predominantly from the *cis,trans** isomer—upon initial excitation of the *cis,cis* analogue—conclusively suggests that the thermodynamic stability of the interconverting stereoisomers is inverted in S_1 with respect to the ground state (S_0). In other words,

Scheme 3. Photodynamic Scheme in Solution for the Lowest Excited State Adiabatic *cis,cis** to *cis,trans** Isomerization of **1** and **2**^a



^a k_1 and k_{-1} are, respectively, the forward and reverse isomerization rate constants in S_1 ; k_A and k_B denote the sum of all rates that deactivate the corresponding excited state both radiatively (k_f) and nonradiatively (k_{nf}) in the absence of isomerization.

the steady-state electronic spectra imply nearly one-way *cis,cis** → *cis,trans** conversion during the lifetime of the excited state (see Scheme 3).

The overall absolute quantum yield Φ and the recovered fluorescence lifetimes of **1** in 2-MTHF as a function of temperature are given in Figure 9. (a) The independence of Φ on wavelength of excitation and (b) the equality of the individual quantum yields and lifetimes of the *cis,cis** and *cis,trans** isomers, i.e., $\Phi_{0,cis,cis} \approx \Phi_{0,cis,trans} = 0.38 \pm 0.02$ and $\tau_{0,cis,cis} \approx \tau_{0,cis,trans} = 8.0 \pm 0.5$ ns (obtained by selective excitation below 260 K), are clearly seen. Moreover, the absence of a measurable temperature effect on Φ over the wide temperature region studied (from 77 to 331 K) clearly demonstrates that a thermally activated nonradiative decay channel is totally absent. Furthermore, no photobleaching was observed upon irradiating the sample continuously. These facts suggest that (a) the isomerization in S_1 is purely adiabatic and (b) the photodynamic cycle is not degraded.

Kinetic Analysis. The photodynamic scheme shown in Scheme 3 can be kinetically analyzed as originally proposed by Barbara et al.^{68–71} for the adiabatic *s-cis** to *s-trans** isomerization of 2-vinyl anthracene. Details are given in the Supporting Information part S6. Briefly, the fluorescence decay intensity $I(t,\lambda)$ can be fitted to a biexponential function of the form

$$I(t,\lambda) = \alpha_1(\lambda) \exp(-\beta_1 t) + \alpha_2(\lambda) \exp(-\beta_2 t) \quad (11)$$

with a short ($\tau_1 = 1/\beta_1$) and long ($\tau_2 = 1/\beta_2$) lifetime component. When the fluorescence decay traces are detected at an appropriate wavelength in which only the A^* (*cis,cis*)* isomer emits (e.g., 346 ± 2 nm), the general solution for the fluorescence intensity $I(t)$ can be expressed as

$$I(t) = k_{f,A} \frac{(X - \beta_2)[A_0]^* - \kappa_{-1}[B_0]^*}{(\beta_1 - \beta_2)} \exp(-\beta_1 t) + k_{f,A} \frac{(\beta_1 - X)[A_0]^* + \kappa_{-1}[B_0]^*}{(\beta_1 - \beta_2)} \exp(-\beta_2 t) \quad (12)$$

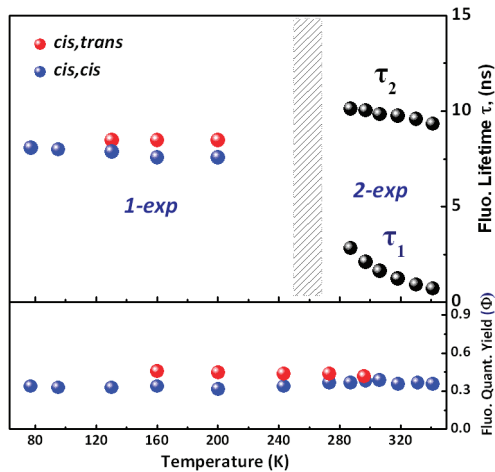


Figure 9. (Top) Lifetimes of the *cis,cis* and *cis,trans* isomers after selective excitation below 260 K (see arrows in Figure 8). Above 260 K, biexponential kinetics was observed (see text). (Bottom) Absolute quantum yields (Φ) at varying temperatures; $\lambda_{\text{exc}} = 337.6 \pm 0.1$ (red circle) and 355.0 ± 0.1 nm (blue circle).

$X = k_A + k_1$ stands for the sum of all rates that deactivate A^* , and B represents the *cis,trans* isomer. By manipulating the preexponential factors quotient $\alpha = \alpha_2/\alpha_1$ and setting $[B_0]^*/[A_0]^* \approx [B_0]/[A_0] \approx K_{\text{eq}}^{\text{SO}} \approx 0.2$, one obtains eq 13 by which the forward rate constant k_1 can be evaluated with an error of $\sim 10\%$

$$k_1 = \frac{1/(1 + \alpha) + K_{\text{eq}}^{\text{SO}}}{1 + K_{\text{eq}}^{\text{SO}}} \left(\frac{1}{\tau_1} - \frac{1}{\tau_2} \right) \quad (13)$$

The analysis of the time-resolved fluorescence decay traces of **1** and **2** in 2-MTHF as a function of temperature indicates the following (see Table 2). First, τ_2 remains independent of temperature and within experimental error is equal to ≈ 10 ns; this provides additional evidence that the excited-state isomerization is purely adiabatic in consistency with the insensitivity of Φ versus T . Second, the recovered excited-state isomerization rate constant ($k_1 + k_{-1}$) is almost independent of exocyclic bulkiness. Third, $k_1 > k_{-1}$, suggesting that the excited-state equilibrium is predominantly shifted toward the *cis,trans** species, as confirmed also by the steady-state fluorescence spectra.

The S_1 activation energies were evaluated from the recovered rate constants in an Arrhenius analysis (see Table 2). In principle $\ln k_{\text{sum}}$ vs $1/T$ should be nonlinear because k_{sum} follows a biexponential form (eq 14).

$$\begin{aligned} k_{\text{sum}} &= k_1 + k_{-1} \\ &= k_1^0 \exp(-E_a^1/RT) + k_{-1}^0 \exp(-E_a^{-1}/RT) \end{aligned} \quad (14)$$

k_1^0 and k_{-1}^0 are Arrhenius frequency factors for the forward and reverse reaction, respectively. The unexpected linearity of the $\ln k_{\text{sum}}$ vs $1/T$ (Figure 10) can be explained considering the fact that the k_1 predominates significantly over the k_{-1} ; that is, the isomerization reaction in S_1 is in fact predominantly one-way, i.e., $k_{\text{sum}} \approx k_1$. The analysis shows that although the compounds **1** and **2** do differ significantly in exocyclic bulkiness they do exhibit nearly identical activation energy for the *cis,cis** \rightarrow *cis,trans** isomerization reaction in S_1 (i.e., forward; $E_a^1 = 20 \pm 1$ kJ/mol and reverse; $E_a^{-1} = 29 \pm 2$ kJ/mol).

Similar results were obtained in methanol and water. This suggests that a solvation and/or proticity effect on the barrier

Table 2. Temperature Dependence of the Observed Lifetimes,^{b,c} Ratio of Preexponential Factors (α_2/α_1), and Recovered Rate Constants^c of **1** and **2** in 2-MTHF, $[1] = [2] = 4.5 \times 10^{-5}$ M^a

1 (2,6-dimethoxytriethyleneglycol naphthalene)						
T, K	τ_1 , ns	τ_2 , ns	k_{sum} , 10^8 s ⁻¹	(α_2/α_1)	k_1 , 10^8 s ⁻¹	k_{-1} , 10^8 s ⁻¹
287	2.93	9.29	2.41	0.24	1.95	0.47
297	2.39	10.03	3.18	0.26	2.53	0.66
306	1.94	9.90	4.14	0.31	3.17	0.97
318	1.54	9.74	5.47	0.37	4.02	1.45
330	1.19	9.50	7.35	0.41	5.27	2.08
341	0.89	9.46	10.20	0.43	7.17	3.03

2 (2,6-dimethoxynaphthalene)						
T, K	τ_1 , ns	τ_2 , ns	k_{sum} , 10^8 s ⁻¹	(α_2/α_1)	k_1 , 10^8 s ⁻¹	k_{-1} , 10^8 s ⁻¹
287	2.84	10.13	2.53	0.26	1.99	0.54
297	2.13	10.06	3.70	0.32	2.80	0.90
306	1.65	9.85	5.05	0.37	3.70	1.35
318	1.25	9.77	6.98	0.43	4.90	2.07
330	0.93	9.60	9.71	0.48	6.63	3.08
341	0.73	9.35	12.63	0.58	8.09	4.54

^a Exc: 337 ± 6 nm. Em: 346 ± 2.0 nm. ^b The statistical parameter χ^2 was between 1.00 and 1.07. ^c Uncertainties in lifetimes and k_{sum} $\sim 5\%$. Uncertainties in preexponential factors and recovered rates $\sim 10\%$.

height in S_1 is not significant. The above findings are quite similar with those obtained in a comparative kinetic and thermodynamic study in S_1 between **1** and **2** when they were dissolved in degassed 3-methylpentane (3-MP) and in the more viscous tetradecane.⁴³ These findings demonstrated that the rate following the adiabatic *cis,cis** \rightarrow *cis,trans** isomerization coordinate was almost independent of exocyclic bulkiness and medium viscosity. Furthermore, correlation of the isomerization rate constants with hydrodynamic friction was found to be completely inconsistent with the prediction of a Kramers-type model that takes into account the isomerization to occur through a volume-demanding *syn* to *anti* exocyclic chain rearrangement (i.e., twisting of the bulky exocyclic group around the $C_{\text{Naph}}-\text{O}$ bond; one-bond flip). All the above facts collectively imply that, at least for **1**, the stereochemical rearrangement following the adiabatic *cis,cis** \rightarrow *cis,trans** isomerization proceeds through a volume-conserving mechanism. This can be principally achieved if the torsional motion is confined to the vicinity of the isomerizing moiety ($C_{\text{Aryl}}-\text{O}-C$). A possible pathway might be the local inversion of the sp^2 hybridized oxygen atom, whereas meanwhile the molecular fragments linked to the inversion center reorient by small amplitude lateral motion (see Scheme 4). This movement is closely related to the lateral motion following the inversion process in the hula-twist mechanism.^{24–29} One cannot exclude, however, that the observed *cis,cis** \rightarrow *cis,trans** transformation is likely the result of BP (crankshaft) motion involving the $C_{\text{Naph}}-\text{O}$ bond coupled with the nearby CH_2-CH_2 single bond (see Scheme 4). Although this motion would achieve a volume-conserving *syn** to *anti** conversion, the results of this work (vide infra) combined with the results obtained from a nonpublished study⁷² do not support the above reaction coordinate.

Before we begin exploring the photoisomerization reactivity of **1** within the restricted tubular space of the assembled β -CDs, it is

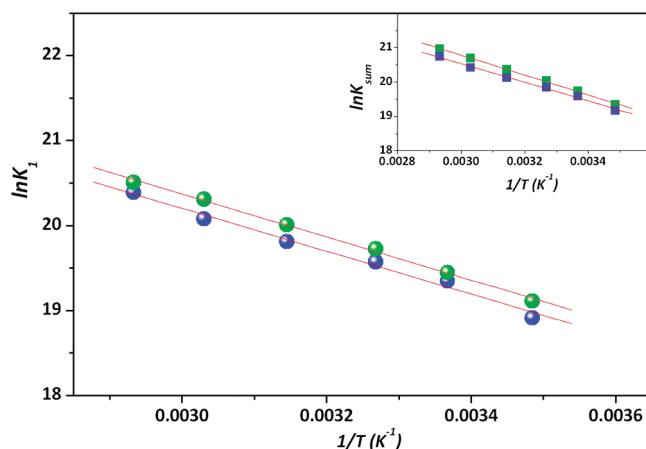


Figure 10. Arrhenius plots for the forward k_1 and (insert) interconversion $k_{\text{sum}} = k_1 + k_{-1}$ isomerization rate constants of compounds **1** (blue circle) and **2** (green circle) dissolved in 2-MTHF.

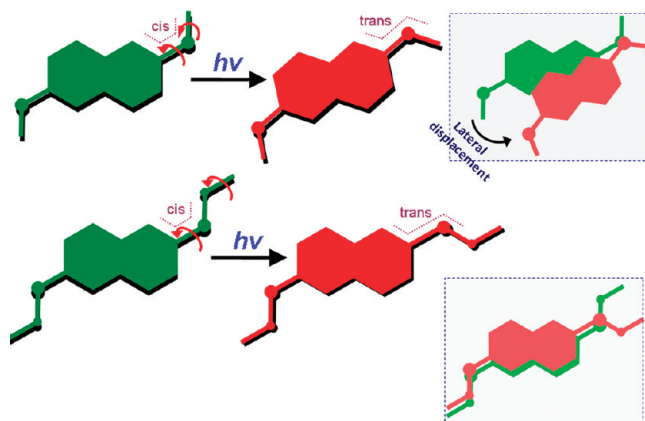
important to review our understanding to this point and anticipate any potential differentiation. First, for both compounds **1** and **2** dissolved freely in a solvent the stable *cis,cis* isomer, upon excitation, is straightforwardly converted in the adiabatic S_1 surface to the closest in energy *cis,trans** analogue. Second, the exocyclic substitution (i.e., the replacement of the methoxy groups of **2** with mTEG chains) as well as environmental stimuli such as solvent's dielectricity, proticity, and viscosity do not appreciably affect (a) the S_1 thermochemistry ($E_a^{S_1} = 20 \pm 1$ kJ/mol in 3-MP, $E_a^{S_1} = 20 \pm 1$ kJ/mol in 2-MTHF and $E_a^{S_1} = 21 \pm 1$ kJ/mol in MeOH) and (b) the absorption and fluorescence spectral positions.

Trans,trans Isomer. The energetically highly unfavorable *trans,trans* isomeric form is predicted to exist in a trace amount in solution⁴⁵ (~1% at ambient conditions in the ground state) and hence cannot be clearly observed spectroscopically. Nevertheless, recently, we were able to trap the above unstable form of **2**—via tight host–guest interactions—within the narrow cavity formed by two assembled α -cyclodextrins (α -CDs) in water.⁷³ The supramolecular complex **2**_trans,trans \subset (α -CD)₂ was permanently stabilized at ambient conditions, thus allowing observation of its own absorption and emission spectra. The 0–0 origins of the above spectra were found to be distinctly shifted bathochromically compared to their counterparts of the *cis,cis* and *cis,trans* isomers (see green colored spectra in Figure 11, bottom).

II. Photoisomerization Reactivity of **1 within the Tubular Cage of the Assembled β -Cyclodextrins.** Figure 11 (bottom) shows the dependence of the absorption spectrum of the predominant *cis,cis* form of **1** (72.0 μ M) in water as a function of added [β -CD] (spectra 1–5). Subtle spectral shifts of ~2 nm are observed, becoming soon saturated at about 3.3 mM β -CD, in consistency with the leveling-off part of the experimental NMR curve, i.e., δH_{Naph} vs [β -CD] (see Figure 1). It is important to note that the absorption spectrum of the caged form of **1** (Figure 11; bottom) coincides with the absorption spectrum of crystals of **1** alone (Figure 11; upper) in which the “fingerprint” of the **1**_cis,cis isomeric form has been manifested by X-ray crystallography.⁴⁵ We recall that the preferential encapsulation of the *cis,cis* isomer of **1** within the interior of the assembled β -CDs has also been supported by the 2D NMR ROESY spectrum.

The photoisomerization reactivity of **1** was followed by fluorescence spectroscopy in the presence of a large excess of β -CD

Scheme 4. Possible *cis,cis** to *cis,trans** Conversion Pathways of Compound **1** in Solution^a



^a Top: Out-of-plane inversion of the oxygen atom. Bottom: Crankshaft motion about two alternating bonds. Insets: Sketches showing the volume requirements imposed by the above structural rearrangements.

(~13.0 mM) to ensure complete encirclement of all chromophoric molecules. Indeed, the absolute fluorescence quantum yield of the engaged **1** was found to be temperature independent and similar to that (~0.40) of degassed solutions⁴³ of **1** (~0.26 in aerated solutions). Moreover, the lifetime of the emitting conformation of **1** increases significantly from ~8.8 ns in non-degassed water to ~14 ns upon encapsulation. The above findings are in very good accordance with the NMR and fluorescence quenching studies and further support insulation and complete protection of the naphthalene subunit within the threaded β -CDs.

Irradiation of the engaged *cis,cis* stereoisomer with continuous light results in a red-shifted fluorescence spectrum, which exhibits an extraordinarily unusual large Stokes' shift of about 25 nm. No photobleaching was observed upon continuous irradiation of the sample. The above suggest the presence of an electronically adiabatic structural rearrangement during the lifetime of the excited state. To explain this unusual observation we have analyzed the time-dependent spectra and the kinetics of the evolution process of the photoproduct in S_1 . When the sample is treated with a pulsed light source, the fully relaxed time-resolved emission spectrum (TRES; i.e., the spectrum obtained when photons are detected with a late delay time >3 ns following pulse excitation) coincides nearly perfectly with the steady-state fluorescence spectrum of the *trans,trans* isomeric form.⁷³ The early gated TRES spectrum (~800 ps after pulse excitation) contains contribution from the initially excited short-lived emitting species, i.e., the *cis,cis** (see Figure 12).

The fact that we see fluorescence from the equilibrium geometry of the formed photoproduct (*trans,trans**) in S_1 —infeasible in *adiabatic* reactions—allows for straightforward evaluation of the kinetic parameters associated with the present novel photoisomerization. To this end, we analyzed the fluorescence decay kinetics as a function of temperature and wavelength of observation. The analysis of the fluorescence decay traces monitored on the long-wavelength side of the main emission band (where it predominantly emits the *trans,trans** photoproduct e.g., 400 nm) follows a biexponential kinetics profile (see Figure 13 and Table 3). It is composed of (i) a component rising in intensity (negative pre-exponential factor) with a short lifetime τ_1 that drastically decreases with increasing temperature and

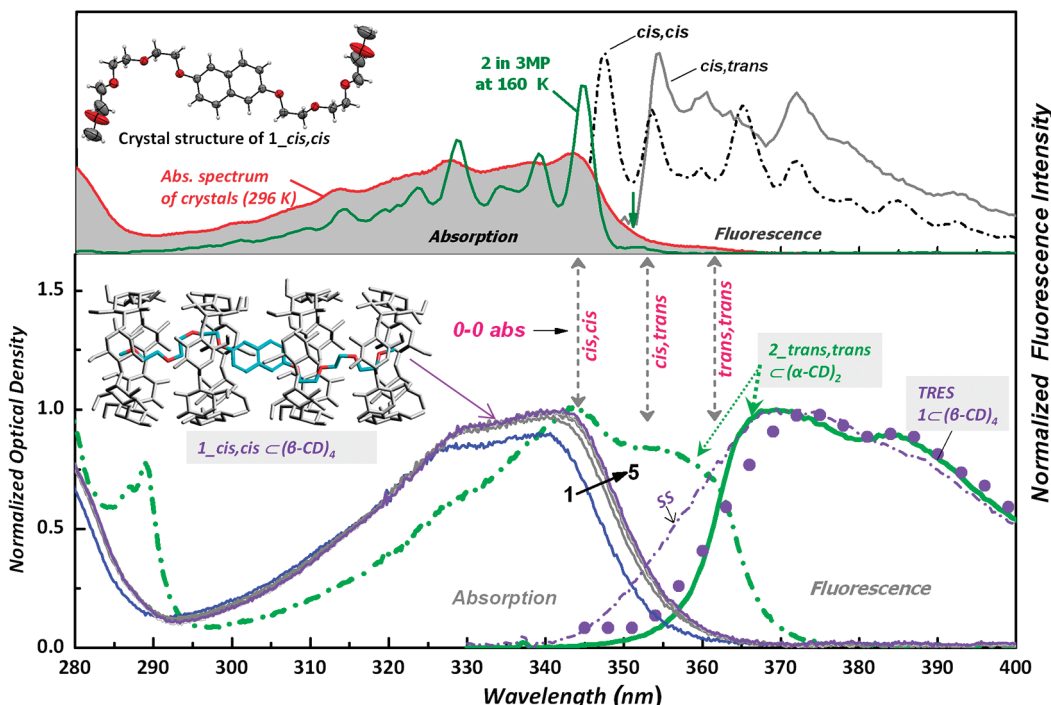


Figure 11. (Top) Left: Absorption spectrum of a crystalline film⁴⁵ of **1**-*cis,cis* and absorption spectra of **2** in 3-methylpentane (3-MP) at 160 K. Right: Pure emission spectra of *cis,cis* and *cis,trans* isomers of **2** obtained at low temperatures (see arrows for excitation). (Bottom) **1** → **5**; absorption spectra of **1** (72.0 μM) in water vs $[\beta\text{-CD}]$; ss is the steady-state fluorescence spectrum of **1** in the fully complexed state (exc: at 337 nm). Green colored curves: Absorption (left) and fluorescence (right) spectrum of the *trans,trans* isomer of **2** trapped within two assembled $\alpha\text{-CDs}$ (exc: at 337 nm). Filled circles: late-gated TRES of **1** in $(\beta\text{-CD})_4$.

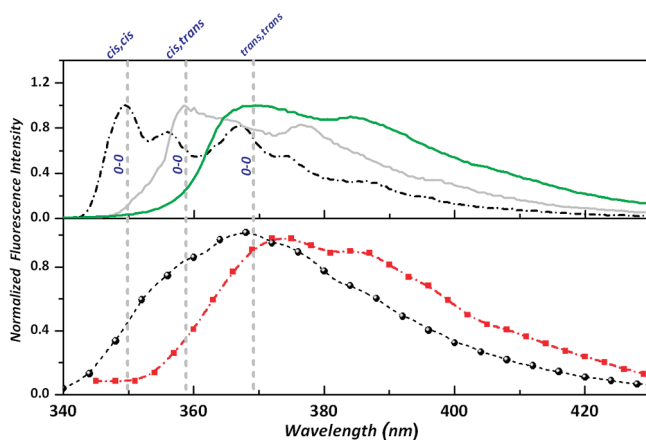


Figure 12. (Top) Pure emission spectra of the distinct isomers of **1** and **2** (see also Figures 8 and 11). (Bottom) Normalized early- (black) and late- (red) gated time-resolved emission spectra of **1** in $(\beta\text{-CD})_4$, observed, respectively, at ~ 800 ps and 3 ns after pulse excitation.

(ii) a subsequent long-lived decaying species with an almost temperature-independent lifetime $\tau_2 \approx 14$ ns. We parenthetically may note that τ_2 is appreciably longer than the intrinsic fluorescence lifetime (~ 10 ns) of the *cis,trans** isomer (the usual S_1 photoproduct in degassed solutions) and confirmatory is closer to the lifetime (16.8 ns) of the *trans,trans* isomer⁷³ of **2** (stabilized supramolecularly inside two assembled $\alpha\text{-CDs}$). At the blue edge of the spectrum, ca. 348 nm, the very weak emission predominantly occurs from the initially excited unreacted *cis,cis** configuration. The decay of the fluorescence intensity is associated

mainly with a short lifetime τ_1 equal to that of the rising in intensity of the *trans,trans** isomer at each temperature employed.⁷⁴

Several interesting features are apparent from these traces. First, the absence of a significant temperature effect on τ_2 indicates that the light-induced isomerization is adiabatic. Second, the photoproduct “grows in” within a short time window equal with that of the decay of the initially excited *cis,cis* isomeric form. This is a manifestation of the photoproduct taking time to form following photogeneration of the *cis,cis** isomer. Third, the fits between the experimental data and the one-way *cis,cis** to *trans,trans** conversion model are very good (see Figure 14).

These results are completely consistent with the presence of only a single maximum which passes along the reaction coordinate. That is, the population of the photochemically generated low-energy species (*trans,trans**) must in fact grow directly in S_1 at the expense of the initially photogenerated *cis,cis* stereoisomer. In other words, the *cis,cis** configuration is the kinetic precursor to the rising *trans,trans** component, which after decaying to the thermal ground state surface returns quickly to the original, energetically stable *cis,cis* configuration. The above photodynamic scheme is illustrated in Figure 15. This novel medium—driven *cis,cis** → *trans,trans** stereospecific transformation (nonpreferred in uninhibited liquids)—could be only explained by considering a volume-saving turning of the naphthalene nucleus about the two quasidouble bonds C_{Aryl}—O by $\varphi \approx 180^\circ$ (see Figure 15b).

The question that arises is *why* doesn't *cis,cis** form *cis,trans** within the cage? We recall again that the above photoconversion is the dominant, low-energy adiabatic isomerization pathway in solution as discussed earlier in this text and elsewhere.⁴³

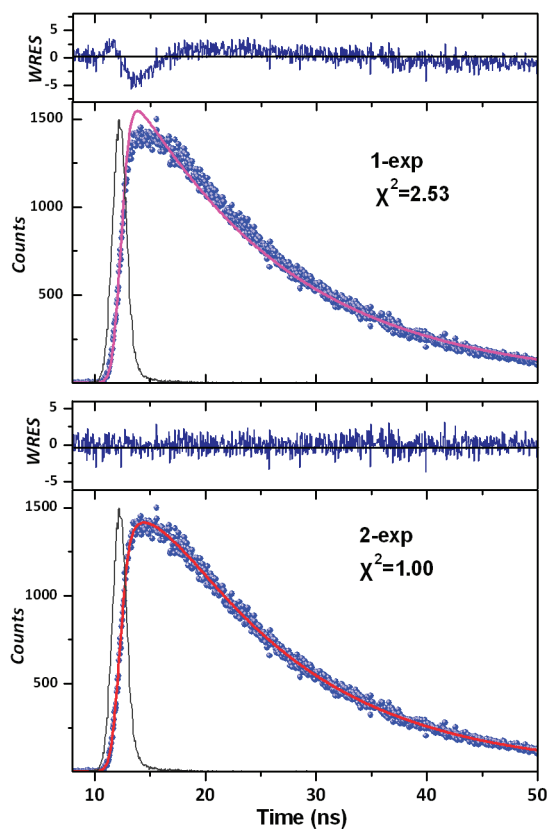


Figure 13. Linear scale, time-resolved fluorescence decay of encaged **1** monitored at 400 nm with mono- and biexponential fitting ($T = 296$ K). The distribution of weighted residuals (WRES) and the χ^2 are also given in both cases.

Table 3. Temperature Dependence of the Fluorescence Lifetimes^a and the Excited-State (S_1) Isomerization Rate Constant^b of **1 within the Treated β -CDs**

T, K	τ_1 , ns	τ_2 , ns	$k_1, 10^8 \text{ s}^{-1}$
287	3.40	14.2	1.99
295	2.89	13.8	2.50
304	2.39	13.2	3.23
315	1.78	12.8	4.67

^a Uncertainties in lifetimes $\sim 5\%$. ^b Obtained using a simplified form of eq 13 for one-way conversion: $k_1 = 1/\tau_1 - k_A$; $k_A \approx 1.0 \times 10^8 \text{ s}^{-1}$.

The answer obviously lies in the particular spatial and cohesive features of the tubular cavity formed by the self-assembled β -cyclodextrins. Responsible for the construction of these features is the elongated body of **1**, which may well serve as a “shaft” to “bunch together” in a face-to-face arrangement of up to four cyclodextrins. This allows each of the secondary cyclodextrin hydroxyls to form a hydrogen bond with a secondary hydroxyl in the adjoining molecule, as exemplified by the X-ray structure shown in Figure 6d and a related β -cyclodextrin-based rotaxane superstructure in the literature.⁵⁵ The above assist the rigid cyclodextrin molecules to be stabilized cohesively through networks of hydrogen bonds, so forming a well-defined and compact tubular nanocage. Thus, the absence of the $cis,cis^* \rightarrow cis,trans^*$ mechanism within the cage may most likely be a consequence of the combination between reduced degree of freedom of the guest

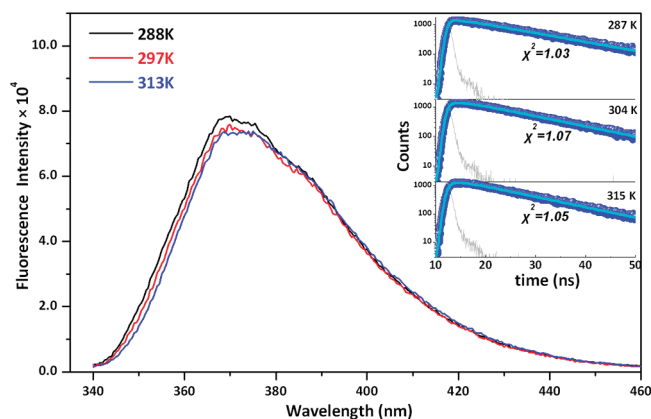


Figure 14. Steady-state fluorescence spectra of encaged **1** at varying temperatures (exc: 337 nm). (Insets) Time-resolved fluorescence decays and best fits (blue lines) at varying temperatures (exc: 337 nm; observation of emission at 400 nm). See Table 3 for the recovered lifetimes.

and stiffness of the tubular body. In effect, if one considers the structural rearrangements associated with the inversion progress (in one of the two sp^2 hybridized oxygens; see Scheme 4), these, albeit volume-conserving, require more space than offered by the interior of the cage. More precisely, the $1-cis,cis^* \rightarrow 1-cis,trans^*$ conversion requires appreciable lateral displacement of the rigid naphthalene subunit to drastically relieve the angle strains imposed by the inversion process (as happens by the closely related hula-twist mechanism^{30–35}). The above motion (nonrestricted in homogeneous liquids) is expected to be sterically hindered inside the cage as (a) the available empty space is limited by the walls of the tube and (b) the cyclodextrin cluster “strength” is great enough to resist against displacement of the CD subunits. In contrast, the direct $1-cis,cis^* \rightarrow 1-trans,trans^*$ conversion does not require any additional molecular rearrangement other than the ring-flipping motion which fits uniquely the available empty space within the tube. It should be noted that the exocyclic crankshaft motion hypothesized in Scheme 4 may also be possible inside the cage. However, the results do not support this motion, as we see no evidence for the $cis,cis^* \rightarrow cis,trans^*$ conversion.

One would assume that the observed $1-cis,cis^* \rightarrow 1-trans,trans^*$ transformation within the cage could occur through the intermediary $cis,trans^*$ form along the adiabatic surface (i.e., $cis,cis^* \rightarrow cis,trans^* \rightarrow trans,trans^*$). This would be possible by sequential absorption of a second photon, e.g., upon continuous irradiation. The possibility of the above evolution, however, should be eliminated, as the results obtained by straightforward kinetic analysis clearly showed the absence of an intermediate trajectory (i.e., the interference of the $cis,trans^*$ isomer). Actually, one-photon excitation with a low-intensity short pulse could not cause the manifestation of two successive inversion processes (i.e., one for each of the separate, centrosymmetrically related exocyclic C_{Naph}—O—C— molecular moieties). In contrast, the one-photon reorientation of the planar aromatic (naphthalene) subunit may be possible, as the “axes” of rotation (i.e., the C_{Naph}—O bonds) constitute the termini of the uniform conjugated length of **1**.

Arrhenius analysis of the barrier-controlled isomerization rate constant in S_1 (Figure 15d) results in $E_a = 23 \pm 1 \text{ kJ/mol}$ and a pre-exponential factor $A \approx 2.6 \times 10^{12} \text{ s}^{-1}$ that is in very good consistency with the frequency calculated from the moment of

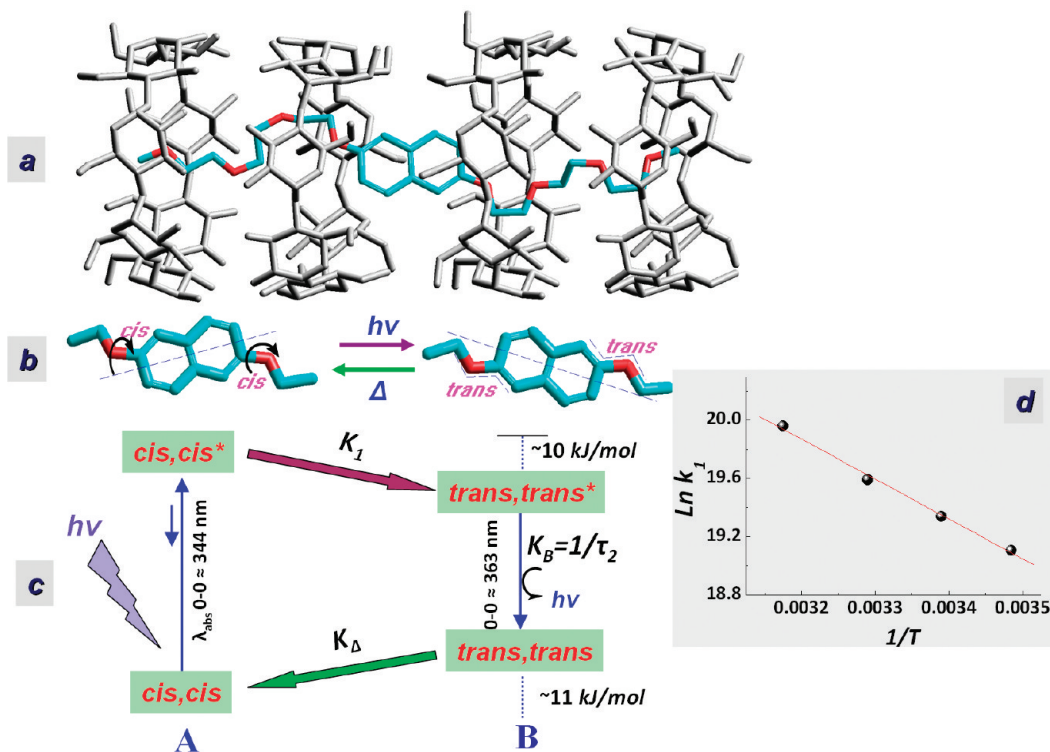


Figure 15. (a) Calculated (RM1; Hyperchem 8.0) superstructure of **1** $\subset (\beta\text{-CDs})_4$. (b) Isomeric forms (core structures) exchanging the rotary component (*cis,cis* and *trans,trans*). (c) Photodynamic cycle. (d) Arrhenius plot for the *cis,cis** \rightarrow *trans,trans** rate constant.

inertia of the naphthalene ring rotating freely about the C_{Aryl}—O links⁷⁵ (1.9×10^{12} s⁻¹).

Although the steady-state and time-resolved results could satisfactorily be explained by a roughly 180° ring flipping of the engaged **1** in S_I, one would be hard pressed to explain why the activation energy ($E_a^{S1} = 23 \pm 1$ kJ/mol) is just barely higher than the activation energy of the typical, low-energy *cis,cis** \rightarrow *cis,trans** conversion observed in solution, e.g., $E_a^{S1} = 20 \pm 1$ kJ/mol in 2-MTHF. Recall that in solution we see no evidence for the competitive coexistence of the above mechanisms. That is, the activation energy of the former mechanism (i.e., *cis,cis** \rightarrow *trans,trans**) should be distinctly higher than that of the latter one.

The manifestation within the cage of lower activation energy than expected may simply be a consequence of the ground state deformation of **1**. That is, distributions of energetically elevated **1** *cis,cis* conformations in which the —C—O—Naph—O—C— dihedral angles deviate from planarity lower the activation barrier for rotation. This is not unexpected considering the fact that conformers in constrained environments can have different torsional angles compared with the gas-phase minimized structures.⁷⁶ For example, gas-phase ab initio calculations⁴⁵ predict that all geometric isomers of **2** should be strictly planar (vide infra), i.e., $\varphi(\text{C}2\text{—C}3\text{—O}1\text{—C}6) = 0^\circ$ or 180° (see Scheme 1). In the crystal structure⁴⁵ of the *cis,cis* form of **2**, however, the above dihedral angles are appreciably deformed by 6.7° due to the crystal packing forces. In the tight interior of the assembled β -CDs, the frustrated *cis,cis* conformation of **1** should be affected in a similar way. This suggestion was further supported by semi-empirical quantum mechanical calculations using either the RM1 or PM3 method for the parametrization of the Hamiltonian as adopted in the HyperChem molecular modeling program version 8.0. Geometric optimizations for both the semiempirical and

ab initio methods (see later in this section) were performed using the Polak–Ribiere conjugated gradient method with a 0.02 kcal/(Å mol) root-mean-squared (rms) convergence limit. More precisely, we have performed geometrical optimizations of **1** within the extended cavity formed by four self-assembled β -CD macrocycles using as input the crystal structure **1** $\subset (\beta\text{-CD})_4$ shown in Figure 6c. Due to the lack of information about the exact conformation of the aromatic core subunit of the **1** *cis,cis* form inside the cage (see X-ray structure; Figure 6c), the conformation derived from the available crystal structure of **1** alone⁴⁵ was initially used as input. Furthermore, the above molecular subunit was guided into the empty tubular space according to the ROESY data (Figure 6b). We tested several possible inclusion geometries by varying slightly each time the position of the aromatic core across the long axis of the tube. In all cases we obtained optimized structures (similar to that shown in Figure 15a) in which the dihedral angles $\varphi(\text{C}2\text{—C}3\text{—O}1\text{—C}6)$ of **1** *cis,cis* $\subset (\beta\text{-CD})_4$ were found to deviate significantly from planarity by $\sim 20^\circ$.

We see no evidence in the absorption spectra of the engaged **1** for the presence in the ground state of the *trans,trans* isomer. Recall again that the presence of this form can be easily detected as is spectroscopically well distinguishable from its isomeric counterparts (its own 0–0 vibronic band at ~ 362 nm is well separated from the 0–0 origins of the lower energy isomers, i.e., *cis,cis* ~ 345 nm and *cis,trans* ~ 353 nm (see Figures 11 and 12)). The absence of the *trans,trans* form in the ground state is not unexpected considering that it is energetically unfavored (the equilibrium geometry of this stereoisomer was predicted to lie around 11.0 kJ/mol higher in energy⁴⁵ than the stable *cis,cis* counterpart). In the ground surface, consequently, the *cis,cis* \rightleftharpoons *trans,trans* thermal equilibrium distribution within the cage is negligible, and thereby the *cis,cis* \rightarrow *trans,trans* thermal hops are

rare. Ab initio calculations using the restricted Hartree–Fock (RHF) in conjunction with the second-order Møller–Plesset perturbation theory (MP2) have been done to obtain the torsional potential-energy profile of the rotation of the naphthalene nucleus about the C_{Naph}–O links⁴⁵ (i.e., *cis,cis* → *trans,trans*) of compound **2** (2,6-dimethoxynaphthalene). Briefly, the torsional potential was evaluated by fixing the dihedral angles φ (C2–C3–O1–C6) of both molecular sides at several values (from 0° to 180° in 20° increments) along the torsional path and relaxing the remaining degrees of freedom.⁴⁵ Geometry-optimized structures and energies of the various conformations of **2** were calculated initially at the RHF/(aug)-cc-pVDZ level, and the output was used as an input for a single-point calculation using the MP2/(aug)-cc-PVDZ procedure. The above method has been demonstrated to be valid for the prediction of rotational barriers in certain conformationally flexible molecules.⁷⁷ The (aug)-cc-pVDZ Dunning correlation-consistent basis set was used as it is well-known that relatively large basis sets improve the accuracy of the calculations.⁷⁸ The two planar conformers *cis,cis*, $\varphi = 0^\circ$, and *trans,trans*, $\varphi = 180^\circ$, were found to be the global minima in consistency with the concept of resonance that is considered as the driving force toward planarity. The maximum of the torsional potential is located at 32.2 kJ/mol with the methoxy groups nearly orthogonal ($\varphi \approx 80^\circ$) to the plane of the aromatic subunit.

The fact that the photodynamic cycle (Figure 15c) is not degraded upon continuous irradiation suggests that once *trans,trans* is formed indirectly (adiabatically through S₁ after photo-generation of the *cis,cis* form) it returns quickly back to the original form (*cis,cis*). The *trans,trans* → *cis,cis* reorientation rate constant k_Δ was estimated to be $7.4 \times 10^8 \text{ s}^{-1}$ (at 295 K) from the Arrhenius equation, $k_\Delta = A \exp(-E_{\text{activation}}^{\text{S}0}/kT)$, using a barrier height of ~21 kJ/mol and the frequency factor A obtained from the moment of inertia of the naphthalene ring rotating freely about the C_{Aryl}–O links⁷⁵ ($1.9 \times 10^{12} \text{ s}^{-1}$).

The experimentally recovered activation barrier in S₁ for the *cis,cis** → *trans,trans** transformation, i.e., $E_a = 23 \pm 1 \text{ kJ/mol}$, is considerably lower than predicted for the counterpart process in S₀. This is not unexpected considering that resonance interactions are considerably larger in S₁ than in S₀. That is, the ordering of the bonds may in fact be reversed in S₁ leading to weakness of the C_{Naph}–O strength, so facilitating the rotation.

Part C. Insights into a Reversible Light–Heat Torque Converter. As long as light can drive simultaneous rotation of two alternating “quasidouble” bonds in S₁, we envision exploring the photodynamic cycle shown in Figure 15c for further exploitation in achieving volume-saving, molecular mechanical response operating continuously. The efforts in the field of light-driven molecular rotary processes adopt bistable systems operating via rotation about the C=C double bond of a rigid molecular sub-unit.^{10–18} Rotation of a bulky molecular group about a C=C axle is spatially a volume-demanding process, and the applicability of these systems may be useful for engineering large-amplitude spatial mechanical motion at the molecular level. Of paramount importance, however, would be the realization of light-driven *volume-saving* turning motions of a specific molecular component in a fully reversible manner. This concept, unexploited so far, lies beyond the above-mentioned conventional one-bond-twist (C=C) photoisomerization scheme and could form the basis for the construction at the molecular level of light-powered torque converters which have components operating reversibly with no volume displacement.

An inspection on the photodynamic scheme (Figure 15c) shows that at equilibrium in the ground state the rings are locked in the *cis,cis* conformation (station A; the *trans,trans* analogue lies ~11.0 kJ/mol higher in energy). In the first excited state, the thermodynamic stability of the above configurations is inverted. This feature along with the absence of branched “waste” photoproducts allows the rotationally mobile group to be diverted along different, energetically downhill tracks during the operation of the photodynamic cycle. The cyclic process can be considered to proceed as follows: At a given temperature, e.g., 295 K, an initial light pulse pushes the system out of the equilibrium state (station A; *cis,cis* configuration) allowing ~85% of the excited molecules to cross over the potential energy barrier of the *cis,cis** → *trans,trans** rotary process ($E_a \approx 23 \text{ kJ/mol}$; rotational frequency ~250 MHz for ~180° ring flipping). The reaction is predominantly one-way and once the *trans,trans** population is formed jumps to the ground state surface local minimum (*trans,trans* configuration; station B) both radiatively and nonradiatively with an overall rate constant $k_B = 1/\tau_2 \approx 7.7 \times 10^7 \text{ s}^{-1}$. The *trans,trans* stereoisomer in the ground surface is energetically highly unstable. Hence, thermal energy from the bath activates a net flux of the rings along an energetically downhill track (fast reorientation of the aromatic rings by ~180°; $k_\Delta \approx 7.4 \times 10^8 \text{ s}^{-1}$ at 295 K; rotational frequency ~740 MHz), and the system returns to its original equilibrium (station A). Importantly, the isomerization is purely adiabatic in S₁. This feature eliminates the presence of undesirable phenomena that could degrade the cyclic process, such as photobleaching or creation of additional ground-state stable photoproducts (unable to reset the original phase) as commonly happen in diabatic photoisomerization reactions. Thus, continuous irradiation can repetitively push the system out of equilibrium allowing reorientation of the rotationally mobile component along successive, energetically downhill diverted tracks to reset the original station without degrading the cyclic process.

In the solid state, the presence of traces (1–2%) of a “frozen” low-energy conformer trapped in the lattice hampers the observation of photoisomerization as energy transfer phenomena become significant. Efforts to improve and develop host–guest systems capable of harnessing volume-preserving motions in the liquid and solid phases are in progress.

CONCLUSIONS

We demonstrate herein a tailored host–guest supramolecular system through which the synchronized motion of two bonds can be realized purely in the excited state to achieve, in conjunction with thermal energy, an otherwise nonpreferred autonomous volume-conserving mechanical response at the molecular level. The host–guest system is composed of (a) a naphthalene ring linked centrosymmetrically—via sp² hybridized oxygen atoms—with methoxytriethyleneglycol chains (**1**) and (b) a nanotubular cage formed by four self-assembled face-to-face β-cyclodextrins threaded onto the long axle of **1**. The results provide clear evidence that the compact cavity completely blocks the photoisomerization pathway manifested in common solution, allowing observation of adiabatic, stereospecific *cis,cis** → *trans,trans** transformation (turning motion of the naphthalene nucleus about the two quasidouble bonds C_{Naph}–O by $\varphi \approx 180^\circ$). The fact that the thermodynamic stability of the isomers is inverted in S₁ with respect to S₀ allows the guest molecule to restore the original (*cis,cis*) configuration by generating torque

thermally, when relaxing to the ground state. We believe that the present system offers insights into how structurally programmed steric relief of selective torsional movements can be controlled supramolecularly to achieve autonomous light-driven, volume-preserving motions.

■ EXPERIMENTAL SECTION

Materials. Solvents were purified as follows: Water was deionized using specially manufactured ion exchange resins, followed by distillation. 2-Methyltetrahydrofuran (2-MTHF) and 3-methylpentane (3-MP) were passed through silica gel and basic alumina (grade I) and then distilled over Na. Methanol was of spectrophotometric grade and used without further purification. D₂O was used without further purification. 2,6-Dimethoxytriethylene-glycol naphthalene (**1**) was synthesized as described elsewhere.⁴⁵ 2,6-Dimethoxynaphthalene (**2**) was purchased from Aldrich and subsequently was purified by vacuum sublimation and recrystallization from a mixture of methanol and chloroform. β -Cyclodextrin (β -CD) was purchased from Cyclolab and recrystallized from water.

Instrumentation and Methods. Absorption spectra were recorded on a Perkin-Elmer Lambda-16 spectrophotometer. Steady-state fluorescence spectra were accomplished by the Perkin-Elmer model LS-50B and the Edinburgh Instruments model FS-900 spectrofluorometer. Fluorescence lifetimes (τ) were determined using the time-correlated single-photon counter FL900, of the above Edinburgh Instruments setup. Details of the temperature-dependent experiments, quantum yield estimations, and fluorescence polarization setup are given elsewhere.^{42,43}

NMR spectra were recorded on a Bruker Avance DRX 500 spectrometer at 500.13 MHz using an inverse broadband probe (BBI) equipped with a z-gradient coil and WXIN-NMR 2.6 software at 298 K. 2D ROESY spectra were acquired using a mixing time of 400 ms. DOSY NMR experiments were carried out as follows: solutions of 4 cm height were used to ensure gradient linearity along the samples. The temperature was controlled using a 535 L/min air flow and kept at 298.0 ± 0.1 K. The measured 90 degree pulses were 10 μ s for the complex and 9.75 μ s for the β -CD alone. A delay $d_1 = 4^*T_1$ (measured $T_1 = 1.16$ s) was used for the measurements, which were carried out with the gradient spin echo sequence *ledbgpspr2s1d* employing a presaturation step. Data were acquired with 32 or 16 scans for each gradient step, 4 dummy scans, a 2.5 ms gradient pulse (δ), a linear gradient of 16–32 steps between 2% and 95%, and diffusion time (Δ) 100 ms. Total acquisition times were 31 or 62 min. Processing was carried out with Bruker's Topspin 2.1 software. Fitting of the diffusion dimension utilized a two-component routine. The reproducibility of the measurements was checked with three repeats for the solution containing the reactants (1 mM **1** and 12 mM β -CD) and two repeats for the free cyclodextrin (12 mM). The width of the 2D DOSY peaks was used to estimate the error of the measurements. The crystal structure of $1 \subset (\beta\text{-CD})_4$ has been deposited at the Cambridge Crystallographic Data Centre and allocated the deposition number CCDC 810233.

All computer fits and simulations, except those of time-resolved experiments, were performed using the commercial available program "Scientist", version 2.01, of Micro Math. This program uses the Powell variant of the Levenberg–Marquardt algorithm providing a numerical solution in minimizing the appropriate function. In a typical ¹H NMR titration experiment, to a solution of **1** (80.0 μ M) in water was added progressively a

solution of β -CD (14.0 mM) containing 80.0 μ M **1** to keep the total concentration of **1** constant throughout the titration, i.e.

$$[1]_{\text{tot}} = [1]_{\text{free}} + [1 \subset \beta\text{-CD}] + [1 \subset (\beta\text{-CD})_2] \\ + [1 \subset (\beta\text{-CD})_3] + [1 \subset (\beta\text{-CD})_4] \quad (15)$$

Combination of the equilibrium law (eqs 1–4) with the balance of mass (eq 15) for the total **1** at any concentration of β -CD during titration can express $[1]_{\text{free}}$ in terms of K_1 , K_2 , K_3 , K_4 , $[1]_{\text{tot}}$, and $[\beta\text{-CD}]$. Substitution into eq 5—with the assistance of eq 5a—gives the master fitting function. For details about parameters settings, see main text in Part A. I. The correlations between the parameters were not significant as indicated by the standard deviations in Table 1.

■ ASSOCIATED CONTENT

S Supporting Information. Experimental details: 2D HSQC, full 2D ROESY, and COSY NMR spectra; excitation-fluorescence anisotropy spectra; crystal structure additional data, and fluorescence kinetic details. This material is available free of charge via the Internet at <http://pubs.acs.org>.

■ AUTHOR INFORMATION

Corresponding Author

*E-mail: pistolis@chem.demokritos.gr.

■ ACKNOWLEDGMENT

We thank Dr. E. Saridakis for X-ray data collection assistance.

■ REFERENCES

- (1) Douhal, A. *Chem. Rev.* **2004**, *104*, 1955–1976.
- (2) Liu, R. S. H.; Hammond, G. S. *Acc. Chem. Res.* **2005**, *38*, 396–403.
- (3) Marconi, G.; Mezzina, E.; Manet, I.; Manoli, F.; Zambelli, B.; Monti, S. *Photochem. Photobiol. Sci.* **2011**, *10*, 48–59.
- (4) Ramamurthy, V. E. *Photochemistry in Organized and Constrained Media*; VCH Publishers: New York, 1991.
- (5) Frutos, L. M.; Andruniow, T.; Santoro, F.; Ferré, N.; Olivucci, M. *Proc. Natl. Acad. Sci. U.S.A.* **2007**, *104*, 7764–7769.
- (6) Schapiro, I.; Weingart, O.; V., B. *J. Am. Chem. Soc.* **2009**, *131*, 16–17.
- (7) Strambi, A.; Durbej, B.; Ferre, N.; Olivucci, M. *Proc. Natl. Acad. Sci. U.S.A.* **2010**, *107*, 21322–21326.
- (8) Saltiel, J.; Papadimitriou, D.; Krishna, T. S. R.; Huang, Z. N.; Krishnamoorthy, G.; Laohhasurayotin, S.; Clark, R. J. *Angew. Chem., Int. Ed.* **2009**, *48*, 8082–8085.
- (9) Altoèa, P.; Cembrana, A.; Olivucci, M.; Garavellia, M. *Proc. Natl. Acad. Sci. U.S.A.* **2010**, *107*, 20172–20177.
- (10) *Molecular Motors*; Schliwa, M., Ed.; Wiley-VCH: Weinheim, 2003.
- (11) Balzani, V.; Venturi, M.; Credi, A. *A Journey into the Nano-world*. In *Molecular Devices and Machines*; Kelly, T. R., Ed.; Wiley-VCH: Weinheim, 2003.
- (12) Kottas, G. S.; Clarke, L. I.; Horinek, D.; Michl, J. *Chem. Rev.* **2005**, *105*, 1281–1376.
- (13) Balzani, V.; Credi, A.; Venturi, M. *Chem. Soc. Rev.* **2009**, *38*, 1542–1550.
- (14) Feringa, B. L. *J. Org. Chem.* **2007**, *72*, 6635–6652.
- (15) Kinbara, K.; Aida, T. *Chem. Rev.* **2005**, *105*, 1377–1400.
- (16) Muraoka, T.; Kinbara, K.; Aida, T. *Nature* **2006**, *440*, 512–515.
- (17) Silvi, S.; Venturi, M.; A., C. *Chem. Commun.* **2011**, *47*, 2483–2489.

- (18) Zheng, Y. B.; Hao, Q. Z.; Yang, Y. W.; Kiraly, B.; Chiang, I. K.; Huang, T. J. *J. Nanophoton.* **2010**, *4*, 1–26.
- (19) Dugave, C.; Demange, L. *Chem. Rev.* **2003**, *103*, 2475–2532.
- (20) Waldeck, D. H. *Chem. Rev.* **1991**, *91*, 415–436.
- (21) Saltiel, J.; Sun, Y.-P. Cis-Trans Isomerization of C,C Double Bonds. In *Photochromism, Molecules and Systems*; Dürr, H., Bounias-Laurent, H., Eds.; Elsevier: Amsterdam, 2003; pp 64–164.
- (22) Saltiel, J.; Charlton, J. L. Cis-Trans Isomerization of Olefins. In *Rearrangement in Ground and Excited States*; de Mayo, P., Ed.; Academic Press: New York, 1980; Vol. III, pp 25–89.
- (23) Liu, R. S. H.; Yang, L. Y.; Liu, J. *Photochem. Photobiol.* **2007**, *83*, 2–10.
- (24) Furukawa, D.; Kobatake, S.; Matsumoto, A. *Chem. Commun.* **2008**, *55*–57.
- (25) Matsumoto, A. *Top. Curr. Chem.* **2005**, *254*, 263–305.
- (26) Odani, T.; Matsumoto, A.; Sada, K.; Miyata, M. *Chem. Commun.* **2001**, *2004*–2005.
- (27) Saltiel, J.; Krishna, T. S. R.; Laohhasurayotin, S.; Fort, K.; Clark, R. J. *J. Phys. Chem. A* **2008**, *112*, 199–209.
- (28) Saltiel, J.; Krishna, T. S. R.; Turek, A. M.; Clark, R. J. *Chem. Commun.* **2006**, *1506*–1508.
- (29) Warshel, A. *Nature* **1976**, *260*, 679–683.
- (30) Liu, R. S. H. *Acc. Chem. Res.* **2001**, *34*, 555–562.
- (31) Liu, R. S. H.; Asato, A. E. *Proc. Natl. Acad. Sci. U.S.A.* **1985**, *82*, 259–263.
- (32) Liu, R. S. H.; Mead, D.; Asato, A. E. *J. Am. Chem. Soc.* **1985**, *107*, 6609–6614.
- (33) Müller, A. M.; Lochbrunner, S.; Schmid, W. E.; Fuss, E. *Angew. Chem., Int. Ed. Engl.* **1998**, *37*, 505–507.
- (34) Yang, L. Y.; Liu, R. S. H. *Photochem. Photobiol.* **2007**, *83*, 1436–1440.
- (35) Yang, L. Y.; Liu, R. S. H.; Boarman, K. J.; Wendt, N. L.; Liu, J. *J. Am. Chem. Soc.* **2005**, *127*, 2404–2405.
- (36) Harada, J.; Uekusa, K.; Ohashi, Y. *J. Am. Chem. Soc.* **1999**, *121*, 5809–5810.
- (37) Conti, I.; Garavelli, M.; Orlandi, G. *J. Am. Chem. Soc.* **2008**, *130*, 5216–5230.
- (38) Khuong, T. A. V.; Nunez, J. E.; Godinez, C. E.; Garcia-Garibay, M. A. *Acc. Chem. Res.* **2006**, *39*, 413–422.
- (39) Gould, S. L.; Tranchemontagne, D.; Yaghi, O. M.; Garcia-Garibay, M. A. *J. Am. Chem. Soc.* **2008**, *130*, 3246–3247.
- (40) Karlen, S. D.; Reyes, H.; Taylor, R. E.; Khan, S. I.; Hawthorne, M. F.; Garcia-Garibay, M. A. *Proc. Natl. Acad. Sci. U.S.A.* **2010**, *107*, 14973–14977.
- (41) Arai, T.; Tokumaru, K. *Chem. Rev.* **1993**, *93*, 23–29.
- (42) Balomenou, I.; Pistolis, G. *J. Am. Chem. Soc.* **2007**, *129*, 13247–13253.
- (43) Balomenou, I.; Pistolis, G. *Chem.—Eur. J.* **2009**, *15*, 4228–4232.
- (44) Albrecht, M.; Bohne, C.; Granzhan, A.; Ihmels, H.; Pace, T. C. S.; Schnurpeil, A.; Waidelich, M.; Yihwa, C. *J. Phys. Chem. A* **2007**, *111*, 1036–1044.
- (45) Balomenou, I.; Kaloudi-Chantza, A.; Bokias, G.; Kallitsis, J. K.; Raptopoulou, C. P.; Terzis, A.; Pistolis, G. *J. Phys. Chem. B* **2010**, *114*, 8181–8190.
- (46) Bolte, M.; Bauch, C. *Acta Crystallogr., Sect. C* **1998**, *54*, 1862–1863.
- (47) Balzani, V.; Gomez-Lopez, M.; Stoddart, J. F. *Acc. Chem. Res.* **1998**, *31*, 405–414.
- (48) Harada, A.; Kamachi, M. *Macromolecules* **1990**, *23*, 2821–2823.
- (49) Harada, A.; Kamachi, M. *J. Chem. Soc., Chem. Commun.* **1990**, 1322–1323.
- (50) Harada, A.; Li, J.; Kamachi, M. *Nature* **1993**, *364*, 516–518.
- (51) Harada, A.; Li, L.; Nakamitsu, T.; Kamachi, M. *J. Org. Chem.* **1993**, *58*, 7524–7528.
- (52) Sauvage, J.-P. *Acc. Chem. Res.* **1998**, *31*, 611–619.
- (53) Wenz, G.; Keller, B. *Angew. Chem., Int. Ed. Engl.* **1992**, *31*, 197–199.
- (54) Wenz, G.; Han, B.-H.; Muller, A. *Chem. Rev.* **2006**, *106*, 782–817.
- (55) Udachin, A. K.; Wilson, D. L.; Ripmeester, A. J. *J. Am. Chem. Soc.* **2000**, *122*, 12375–12376.
- (56) Pistolis, G.; Malliaris, A. *J. Phys. Chem.* **1996**, *100*, 15562–15568.
- (57) Pistolis, G.; Malliaris, A. *J. Phys. Chem. B* **1998**, *102*, 1095–1101.
- (58) Cameron, K. S.; Fielding, L. J. *Org. Chem.* **2001**, *66*, 6891–6895.
- (59) Guerrero-Martinez, A.; Gonzalez-Gaitano, G.; Vinas, M. H.; Tardajos, G. *J. Phys. Chem. B* **2006**, *110*, 13819–13828.
- (60) Lackowicz, J. R. *Principles of Fluorescence Spectroscopy*, 3rd ed.; Plenum Press: New York, 2006.
- (61) Roi, M.; Doraiswamy, S. *J. Chem. Phys.* **1993**, *98*, 3213–3223.
- (62) For a prolate ellipsoid, if the absorption and emission transition moments are collinear and polarized vertically to the long symmetry axis of the ellipsoid, the anisotropy in fact decays with two correlation times. The one is related with rotation about the long (unique) axis of the ellipsoid. This motion is very fast and displaces the transition moments within a couple of picoseconds leading to a rapid randomization about the major axis (α). The other correlation time is associated with the much slower rotation about one of the other two equivalent minor axes (b) and reflects for the tumbling motion of the ellipsoid. The instrumental setup used here can resolve only the slow decay anisotropy component which in essence carries out the information about the size and shape of the rotating supramolecular entity. We should also note that the analysis made in Figure 4 refers to the intensity decay of the *trans,trans** isomer which is photogenerated in S1 after exciting the stable *cis,cis* isomer. As the *cis,cis** → *trans,trans** conversion is followed by a ~1800 ring flipping about the long axis of the ellipsoid, the transition moment remains approximately on the minor axis. The above can also explain the reduced value of the fundamental anisotropy extracted from the fit ($r_0 \sim 0.14$) which is in good agreement with the anisotropy decay law $r = 0.10 \exp(-t/\tau_r)$ predicted by theory for the slow rotating component.
- (63) Balomenou, I.; Pistolis, G. *J. Phys. Chem. B* **2006**, *110*, 16428–16438.
- (64) Balabai, N.; Linton, B.; Napper, A.; Priyadarshy, S.; Sukharevsky, A. P.; Waldeck, D. H. *J. Phys. Chem. B* **1998**, *102*, 9617–9624.
- (65) Tormo, L.; Organero, J. A.; Douhal, A. *J. Phys. Chem. B* **2005**, *109*, 17848–17854.
- (66) Because compound **2** is sparingly soluble in water, a solution of 50/50 v/v of methanol/water was used.
- (67) In the fluorescence spectrum at ambient temperatures, the 0–0 vibronic band at ~358 nm for *cis,trans** has been decreased in relative intensity with respect to 0–1 (~368 nm). The evolution of this change was observed in the fluorescence spectrum above 200 K and through ~260 K. Moreover, the fluorescence lifetime was increased slightly to ~10 ns, and notably a delayed rise of the fluorescence was not observed at all. The absorption spectra showed that the abruptness of the thermal transition is not due to the creation of the *trans,trans* isomer in the ground state. Most likely, the evolution observed in the 0–0/0–1 ratio between 200 and 260 K is due to a thermally activated conformational distortion.
- (68) Barbara, P. F.; Janeba, W. *Acc. Chem. Res.* **1988**, *21*, 195–199.
- (69) Brearley, A. M.; Flom, S. R.; Nagajan, V.; Barbara, P. F. *J. Phys. Chem.* **1986**, *90*, 2092–2099.
- (70) Brearley, A. M.; Stanjord, A. J. G.; Flom, S. R.; Barbara, P. F. *Chem. Phys. Lett.* **1985**, *113*, 43–48.
- (71) Flom, S. R.; Nagajan, V.; Barbara, P. F. *J. Phys. Chem.* **1986**, *90*, 2085–2092.
- (72) The fact that we observe very similar spectroscopic and kinetic manifestations in solutions of varying viscosities between **1** and its analogue **2** (dimethoxynaphthalene, in which the pedal coordinate CNaph—O—CH₂—CH₂ obviously is not available) conclusively implies that the exocyclic “crankshaft” motion is nonpreferred. This view was strengthened by experiments in which the isomerization kinetics of **1** and **2** was studied in the highly viscous ethyleneglycol solvent ($\eta_{\text{Glycol}} = 17 \text{ cP}$). The results showed that the excited state isomerization rate constant for **1** was diminished by a factor ~1.8 compared to that of the derivative **2**. This is in contrast to what is expected for the crankshaft motion in **1** since this motion does not require appreciable displacement of solvent molecules compared to the more volume-demanding isomerization

pathway of the methoxy group (i.e., the OBF or the lateral movement imposed by the inversion process).

- (73) Balomenou, I.; Pistolis, G. *J. Phys. Chem. B* **2010**, *114*, 780–785.
- (74) The emission intensity at 345 ± 2 nm is very weak, and the analysis of the decays reveals an additional minor component ($\sim 30\%$) of ~ 10 ns. This most probably is due to the presence in the sample of traces of the complexed **1-cis,trans** isomer.
- (75) Kawski, A. *Crit. Rev. Anal. Chem.* **1993**, *23*, 459–529.
- (76) Bernstein, J. *Polymorphism in Molecular crystals*: Oxford University Press Inc.: New York, 2002.
- (77) Abu-Eittah, R. H.; Khedr, M. K. *J. Mol. Struct. (Theochem)* **2007**, *822*, 74–79.
- (78) Pérez-Jiménez, Á. J.; Sancho-García, J. C.; Pérez-Jordá, J. M. *J. Chem. Phys.* **2005**, *123*, 134301–134310.